The safety of masonry arches with uncertain geometry

N. Cavalagli, V. Gusella, L. Severini*

Department of Civil and Environmental Engineering, University of Perugia, Italy

Abstract

This paper aims to evaluate the effect of the geometrical uncertainties on the collapse condition of the circular masonry arch in presence of horizontal actions. Adopting Heyman's hypotheses about the material, a limit analysis based procedure has been developed in order to evaluate the horizontal loads multiplier, taking into account the uncertainties related to the imprecisions of construction, the shape defects of the voussoirs or the deterioration level. The collapse state has been determined in terms of horizontal loads multiplier, whose statistical moments up to second order and probability density functions have been evaluated versus a stereometry parameter. The comparison between the obtained results and those related to the nominal geometry highlighted that the uncertainties effects could reduce significantly the nominal bearing capacity of the structure. Within this context, a safety factor, which takes into account such effects, is introduced.

Keywords: Masonry arch, Uncertain geometry, Limit analysis, Collapse mechanism, Seismic action.

1. Introduction

The cultural and architectural heritage in seismic areas often shows a high vulnerability, requiring a special attention in order to ensure its protection and conservation. Many ancient structures are characterized by the presence of the masonry arch as bearing element, since it was one of the first structural solutions to be thought in order to carry loads. Although the arches

*Corresponding author

Email addresses: nicola.cavalagli@unipg.it (N. Cavalagli), vittorio.gusella@unipg.it (V. Gusella), lauraseverini@strutture.unipg.it (L. Severini)

and vaults have already been known, the credit to understand the potential of these elements goes to the Romans. The architect Vitruvius, in his famous book De Architectura, proves to have a deep knowledge of the thrust exercised by arches or vaults. The Romans consolidated the constructive practice by using the arch for the bridges and aqueducts construction, determining in this way the development of the infrastructure network. Starting from the Middle Age and passing through the Renaissance, the construction technique of the masonry arches led to architectural masterpieces that were designed according to stability criteria, although at the time a clear static or mechanical justification had not yet been provided. When designing a masonry structure, both the medieval masters and then the architects of Humanism and Renaissance referred to their system of practical rules, jealously guarded. Some of them can be traced in ancient treatises, whose derivation is often unknown, since they belonged to the heritage of secret knowledge passed down from one generation of builders to the subsequent one. The design was carried out by establishing precise rules of proportion between the structural elements of the building: the equilibrium state was achieved through geometrical criteria, without any consideration of the concepts of statics, strength, safety and collapse loads [1]. This *geometrical approach* was almost abandoned during the XIX century and the favourite key to reading the behavior of the masonry arches became the elastic analysis. However, the scientific community of that time became soon aware of the ephemeral nature of the state of a masonry structure and of its close relationship with the arbitrary definition of the boundary conditions. During the second half of the XX century the plastic theory spread among the scientists and became parallel with the elastic one; the limit analysis, strongly connected to geometry, started to be considered as a valid method for the structural analysis of the masonry arches. For a detailed analysis on the historic development of the static theories on masonry arches, the reader is invited to see [2, 3].

In particular, since the beginning of the studies on the stability of masonry arches through the limit analysis, carried out for the first time by Jacques Heyman during the XX century, the bearing capacity of these structures has been considered a geometric problem [4, 5]. The research on the optimal shape and the minimum thickness has been a central topic for years and is still now a theme of great interest, both for the specific case of an arch [6, 7, 8] and for vaults and dome more in general [9, 10, 11, 12]. In particular, the first solution for the minimum thickness of the circular masonry arch was provided by Milankovitch about one century ago; an interesting remark can

be found in [13, 14].

Some studies have been developed regarding the effects of the stereotomy on the collapse loads multiplier. The term stereotomy – from the Greek στερεός, solid and τομή, cut – refers to the science of the cutting of solids and uses the geometrical projections for the determination of the shape and size of the stones that form arches, vaults or domes.Differently from the main contributions that considered an arch made of voussoirs having constant thickness and joints defined by radial cuts, more recently, other authors studied the effect of a non-radial joints orientation on the minimum thickness of the arch [15], revealing that the thrust line is not unique since it depends on the shape of the voussoirs.

The effect of an irregular geometry on the bearing capacity of masonry arch bridges has been studied by de Arteaga *et al.* [16], through the Livesley's linear programming method combined with a detailed structural relief, performed by means of planimetric surveying techniques. The results, related to some cases study subjected to the action of a vertical pointed load, permitted to highlight that an idealized geometry may lead to an unsafe solution in term of collapse multiplier. The main influence of the thickness value on the collapse condition of the masonry arch has been highlighted by Riveiro *et al.* [17, 18], who applied a limit analysis based procedure to an existing masonry arch bridge, whose geometry has been reconstructed in detail through a novel methodology for the three-dimensional survey [17], subsequently improved by means of an integration with non-destructive tests for the geometrical characterization of the hidden portions of the structure [18]. The influence of a local thickness reduction on the seismic capacity of masonry arches has been evaluated by Zampieri *et al.* [19] by means of a limit analysis procedure based on the virtual work principle. The parametric analysis on the characteristics of the defect has shown a variation of the collapse multiplier value and of the collapse mechanism, depending on the intensity and localisation of the defect itself. The effects of a localized thickness loss of the arch has been analysed also by Zanaz *et al.* [20], who presented a methodology for the assessment of the masonry vaults bearing capacity in presence of a pointed vertical load, based on the finite element method. All these approaches consider the irregularity of the structure by means of the regeneration of its real geometry or through the identification of a local defect, but they do not reproduce the uncertainty related to the shape of each constitutive stone element of the arch. When the analysis reveals that the structure is not able to stand the assigned loads, strengthening interventions

should be realized in order to increase its bearing capacity [21, 22, 23, 24].

The knowledge of the carrying capacity under horizontal loads is a first fundamental step toward the comprehension of the behaviour of complex structural systems in seismic areas. When evaluating the limit equilibrium condition of the masonry arch, the presence of both vertical and horizontal loads has been considered by several authors [25, 26, 27, 28, 29, 30], also with the presence of the backfill for the analysis of historical bridges [31, 32]. In this context, the evaluation of the ultimate resistance of the masonry arch has been usually carried out by considering deterministic values of the involved geometrical or mechanical parameters, but actually many factors can affect the deterministic ideal bearing capacity. The effects of the random variability of the material strength have been evaluated by some researchers for the circular masonry arch subjected to vertical loads, through static or kinematic approaches [33, 34]. Other studies have been carried out on masonry arch bridges subjected to vertical pointed loads, in order to perform a safety assessment that takes into account the random variability of the properties of the backfill [35]. A probabilistic approach for the safety assessment of existing arches has been proposed by Schueremans *et al.* [36] and applied to a circular masonry arch having an uncertain geometry and subjected to a vertical pointed load. Defects on the shape of the voussoirs, due to both the imprecisions of construction and the deterioration associated to environmental actions, can often be found in masonry structures. Hence, the safety assessment of the masonry arch should take into account the variability of these factors, by adopting random values of the geometrical parameters instead of deterministic ones. To the knowledge of the authors, there are no studies about the effects of the geometrical uncertainties of the voussoirs on the collapse load of the masonry arch in presence of horizontal actions. In fact, the existing studies took into account only the presence of vertical loads or considered the real geometry of a certain case study, without reproducing the uncertain geometry of each voussoir in a probabilistic sense.

This paper deals with the uncertain geometry and its effects on the horizontal loads carrying capacity of the circular masonry arch. In the first part of this work, the limit analysis based procedure has been explained and a deterministic calculation, which refers to an ideal geometry, has been carried out in order to determine the nominal horizontal loads multiplier. Nowadays, other computational methods could be useful to carry out consistent numerical analyses, taking also into account the effective behaviour of the materials, with their hardening and softening response. Nevertheless, when

a significant amount of cases has to be considered, the limit analysis is an efficient tool, which allows to achieve reliable results with low computational costs. The evaluation of the failure condition has been performed by adopting the well known Heyman's hypotheses related to the masonry, which has been considered as a no-tension material, with infinite compressive strength and capable to generate a friction between the voussoirs that prevents the sliding. In the second part, the effects of the geometrical uncertainties of the voussoirs and the imprecisions of construction have been modelled. Among the approaches that could be used to analyse the uncertainties effects on the structural response, probabilistic, fuzzy and interval methods are worthy of note [37]. The fuzzy method is generally used when the boundaries of a set of activities are not well-defined [38], while the interval method can be used when the uncertain parameters are denoted by simple ranges. However, even if the analyses performed in this work are based on the variability of some parameters within specific ranges related to geometric tolerances, the probabilistic approach has been preferred due to the great number of variables to be considered, for example in the case of high number of voussoirs. In fact, the thickness, the radius of the mean circular construction line of the arch and the angle of embrace of each voussoir have been considered as random variables with uniform probability density functions. All the other parameters involved in the problem have been taken into account as deterministic. The effects of the uncertain geometry on the horizontal loads carrying capacity have been evaluated in term of probability density function of the horizontal load multiplier.

2. Mechanical model and limit analysis

2.1. The limit analysis based method

The safety of the masonry arch has been analysed by referring to the limit analysis. A thrust line analysis has been carried out starting from the following hypotheses for the masonry: *i*) no-tension material, *ii*) infinite compressive strength and *iii*) the sliding between the voussoirs does not occur. The applied method is based on the assumption that the arch at the collapse satisfies at the same time the equilibrium, the resistance criterion and the mechanism condition. In other words, the thrust line must be determined by imposing the equilibrium respect to the acting loads, including the self-weight, and must be contained everywhere inside the thickness of the arch in order to make the resistance criterion satisfied. The mechanism condition

requires that the thrust line passes tangent to the boundaries of the masonry at the intrados and extrados in correspondence of a certain number of points, determining the growing of hinges that turn the structure into a kinematic chain. The rotational mechanism is characterized by a number of hinges depending on the geometry of the arch and the loading system [29].

2.2. Nominal geometry

The circular masonry arch in its plane has been considered. The deterministic geometry – in the following indicated *nominal geometry* – of the structure has been defined by assigning the radius R, the angle of embrace α and the thickness t. The total arch length has been denoted by $\delta = R\,\alpha$. The arch has been discretized into n voussoirs by radial lines passing though the centre O (Fig. 1), so that the values of the angle of embrace of each voussoir $\alpha_i = \alpha/n$ and the corresponding subtended arch length $\delta_i = \delta/n$ have been defined, with $i = 1$ to n. The position of each joint has been identified through the progressive angle

$$\beta_j = \frac{\pi - \alpha}{2} + (j-1)\,\alpha/n, \quad \text{with} \quad j = 1 \dots n+1 \tag{1}$$

Assuming radial joints, the arch stereotomy is deterministically defined (any voussoir is an arch of ring with radial initial and final section). On the other hand, varying the number of the voussoirs, it appears adequate to introduce a stereometry parameter, from the Greek στερεός, solid and μέτρον, measurement. Let us define the stereometry parameter

$$\eta = \frac{\alpha}{n} = \frac{\delta}{R\,n} \tag{2}$$

that can have two meanings: the effective microstructure of the arch and the discretization adopted in the numerical structural analysis.

2.3. Loading system

Dealing with the seismic actions, the generic masonry arch analysed in this paper has been subjected to the action of the self-weights of the voussoirs F and to a system of horizontal loads F_S proportional to the weights through a load multiplier k, both applied at the centre of mass G of each voussoir (Fig. 2). Hence, the vertical component of the seismic action has not been taken into account, even if its contribution could play a significant role in the stability assessment of masonry arch-type structures. However,

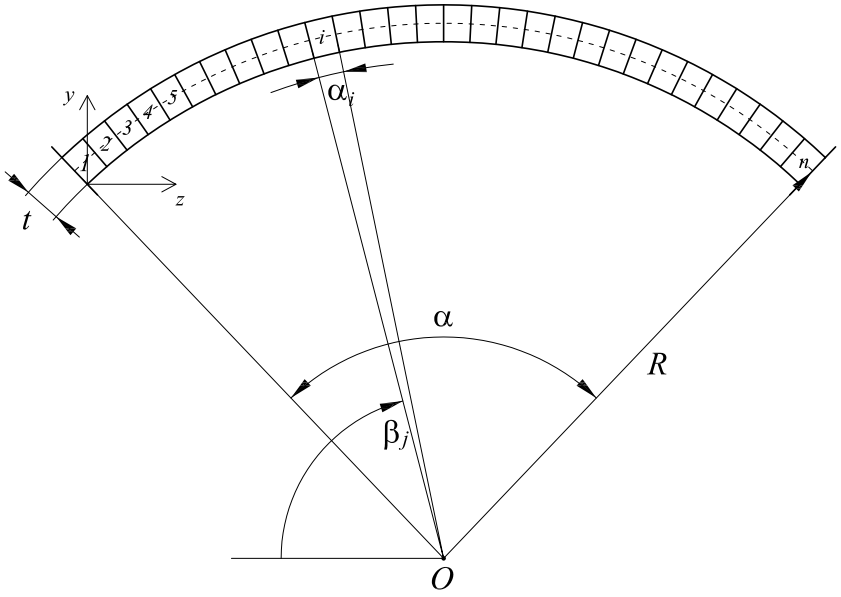

Figure 1: Nominal geometry of the masonry arch.

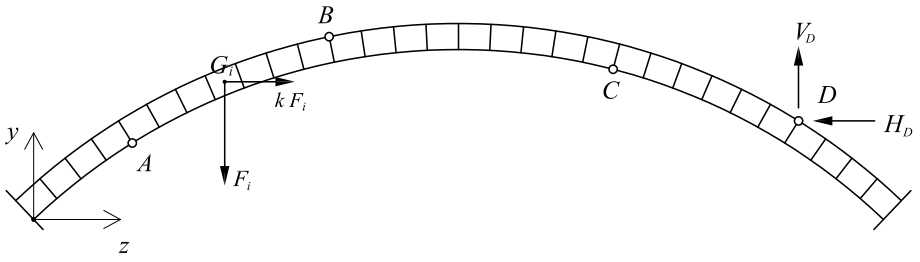

Figure 2: Loading system and generic configuration of the hinges at the collapse.

in order to compare the results obtained by the proposed procedure with those reported in several papers already present in the literature, the only horizontal component has been considered which is related to the vertical weight through a constant multiplier. In fact, according to several works [25, 27, 26, 39, 28, 40, 29], being the structure modelled as a rigid body, it is reasonable to consider that, at the collapse, the lateral inertial load for each voussoir is proportional to the vertical distribution of the mass by means of the same load multiplier k, related to the level of horizontal ground motion acceleration. Indeed the loading system applied to the ith voussoir consists of:

$$F_i = \rho_m \, A_i \, d \tag{3}$$

$$F_{S_i} = k \, F_i \tag{4}$$

where ρ_m is the specific weight of the masonry, A_i the area of the ith voussoir and d the out-of-plane depth of the arch, assumed unitary. The horizontal loads have been assumed directed from left to right. The asymmetric loading condition, due to seismic loads, implies that a four-hinges mechanism forms at the collapse.

2.4. Numerical procedure

The evaluation of the horizontal loads multiplier k has been carried out by following the iterative procedure briefly described below. Let us denote by A, B, C and D the four collapse hinges and by V_D, H_D the reactions at hinge D (Fig. 2). A first attempt position of the collapse hinges has been assumed, corresponding to values of the progressive angles equal to β_A, β_B, β_C and β_D. The equilibrium of the rigid blocks AD, BD and CD has been imposed respectively around the hinges A, B and C, providing the following system of equations:

$$\begin{cases} H_D(y_C - y_D) + V_D(z_C - z_D) - \sum_{i=1}^{n_{CD}} F_i(z_C - z_{G_i}) - k \sum_{i=1}^{n_{CD}} F_i(y_C - y_{G_i}) = 0 \\ H_D(y_B - y_D) + V_D(z_B - z_D) - \sum_{i=1}^{n_{BD}} F_i(z_B - z_{G_i}) - k \sum_{i=1}^{n_{BD}} F_i(y_B - y_{G_i}) = 0 \\ H_D(y_A - y_D) + V_D(z_A - z_D) - \sum_{i=1}^{n_{AD}} F_i(z_A - z_{G_i}) - k \sum_{i=1}^{n_{AD}} F_i(y_A - y_{G_i}) = 0 \end{cases} \tag{5}$$

where n_{AD}, n_{BD} and n_{CD} represent the number of voussoirs between hinges A, B, C and the hinge D. Once the system of equations (5) is solved, the loading system is completely known. Hence, the thrust line can be determined by evaluating the eccentricity e_j of the normal force in correspondence of each joint. The satisfaction of the resistance criterion is then checked:

$$-\frac{t}{2} \leq e_j \leq \frac{t}{2} \tag{6}$$

Eq. (6) must be verified at each joint, by considering the sign of equality only at the hinges joints, in order to obtain the actual horizontal loads multiplier k and the corresponding collapse mechanism. On the contrary, if the resistance criterion is not satisfied, a new attempt configuration of hinges has to be assumed and the calculation repeated. For a more detailed description of the procedure, the interested reader is invited to see [29].

2.5. Horizontal loads carrying capacity for nominal geometry

In the first part of this work, the limit analysis of the circular masonry arch has been carried out by considering the nominal values of the geometrical parameters. Following seminal works taken from the literature (e.g. [27]), the results related to a circular arch with a unitary radius R, an angle of embrace α equal to 157.5° (2.7489 rad) and a thickness-radius ratio t/R of 0.15 will be shown. In order to obtain a solution for the discretized arch which is equivalent to that of the arch made of a continuous mean, a high number of voussoirs should be adopted [29].

Let us denote by k_{nom} the nominal horizontal loads multiplier corresponding to a continuous solution and by k_η the horizontal loads multiplier obtained through a discretization of the structure with n voussoirs, or equivalently

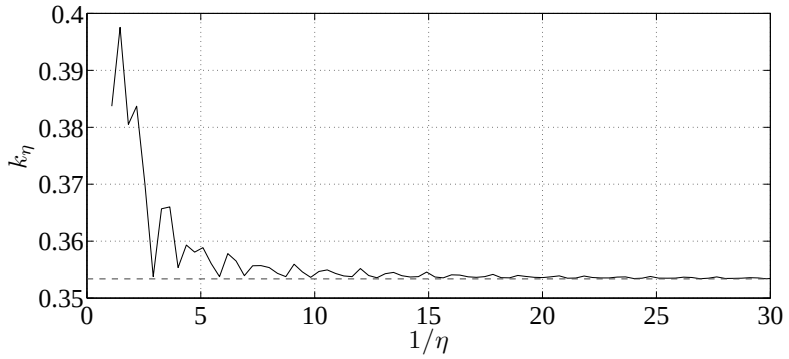

Figure 3: Horizontal loads multiplier k_η (continuous black line) and nominal multiplier k_{nom} (dashed blue line) for the analysed arch depending on the stereometry parameter.

with a stereometry parameter η. In order to highlight the influence of the discretization, a sensitivity analysis has been carried out by varying the stereometry parameter η and evaluating the corresponding value of the horizontal loads multiplier k_η. The results have been represented in Fig. 3 through a continuous black line linking the values k_η. The results show a high variability of the horizontal loads multiplier in the range of low values of $1/\eta$, while if $1/\eta$ increases the horizontal loads multiplier tends to a limit value, which can be defined as the nominal horizontal loads multiplier k_{nom} (horizontal dashed blue line of Fig. 3). Hence, it results:

$$k_{nom} \leq k_\eta \tag{7}$$

This observation, related to an assigned arch geometry, has a general validity when a deterministic approach is adopted. The solution k_η depends on the number of voussoirs and differs, in general case, from the exact multiplier obtained through a continuous analysis. The coincidence of the two values can be obtained through a reduction of the stereometry parameter, i.e. by increasing the number of voussoirs:

$$k_{nom} = \lim_{n\to\infty} k_\eta = \lim_{\eta\to 0} k_\eta \tag{8}$$

Eq. (7) can be proved through the kinematic theorem of the limit analysis. In fact, as a consequence of the discretization, the hinges may develop in different positions respect to those of the continuous solution and the cor-

α [rad]	R [m]	t/R -	k_{nom} -	β_A [rad]	β_B [rad]	β_C [rad]	β_D [rad]
2.7489	1	0.15	0.3534	0.2238	1.2318	2.2397	2.9452

Table 1: Data and results of the deterministic limit analysis.

responding horizontal loads multiplier is, therefore, a kinematic multiplier. The kinematic multiplier may be equal to the collapse multiplier of the continuous system – i.e. k_{nom} – for particular discretizations, corresponding to the stereometry parameter $\overline{\eta}$, that permit the formation of the hinges in positions very close to those obtained by the continuous solution [40]. For what concerns the practical implementations, Eq. (7) highlights the safety of any continuous solution for the limit analysis of the masonry arch with nominal geometry.

In order to evaluate the nominal results in term of horizontal loads multiplier and position of collapse hinges, a number n of voussoirs equal to 300, corresponding to $\eta = 0.0092$, has been used for the masonry arch considered in this paper. In Tab. 1 the data and the results of the deterministic analysis are summarized, being α the fixed value of the angle of embrace of the arch, R the radius of the mean circular construction line, t the thickness and β_A, β_B, β_C and β_D the progressive angles of the four collapse hinges. In Fig. 4 the thrust line referred to the nominal condition has been depicted, highlighting the position of the collapse hinges.

It should be noted that in the previous analyses, and then also in the following, no restriction has been assumed for the number of voussoirs, which could be either even and odd. This hypothesis implies that no specific attention has been devoted to the presence or not of a keystone, because the four-hinges collapse mechanism related to the vertical and horizontal forces does not involve the central joint, except in the cases of very low number of voussoirs. In other words, the presence of the keystone does not change the main results of this work.

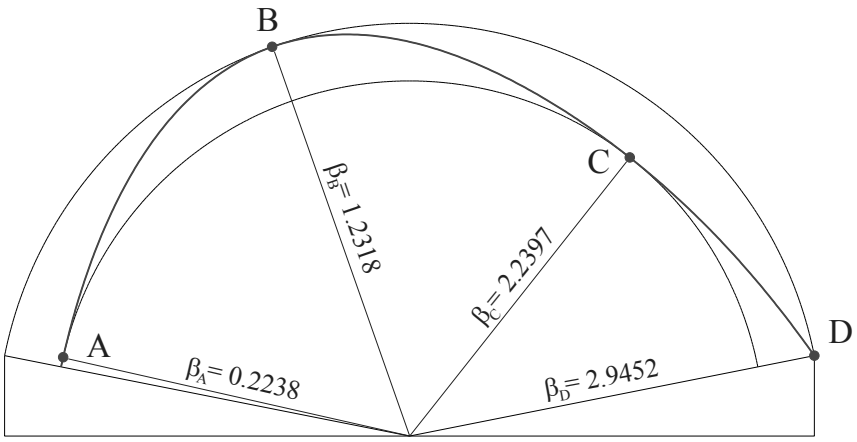

Figure 4: Nominal thrust line and collapse hinges resulting from a high discretization ($n = 300$).

3. A probabilistic approach

3.1. Definition of the uncertain geometry

A deterministic approach is currently adopted in the limit analysis. In fact, all the parameters involved in the calculation are usually considered to be exactly known. Actually, the obtained solution in terms of horizontal loads multiplier and collapse mechanism is an approximation of the effective one. This could be due to many causes, such as shape defects of the voussoirs, imprecisions of execution or material deterioration due to environmental actions. Hence, in the framework of the safety assessment of masonry structures, a probabilistic analysis should be adopted to take into account these aspects and to ensure that the bearing capacity is not overestimated.

The uncertain geometry of the masonry arch has been modelled by assuming the following hypotheses: *i*) radial joints, *ii*) nominal value of the angle of embrace α of the arch and *iii*) uniform probability density functions for the random geometrical parameters (independent functions). Three nominal parameters, which have been previously defined with reference to the entire structure and considered constant at §2.5, in this section have to be related to each voussoir: α_i, t_i and R_i denote respectively the angle of embrace, the thickness and the radius of the mean circular construction line associated to the generic ith voussoir. In the nominal condition it results:

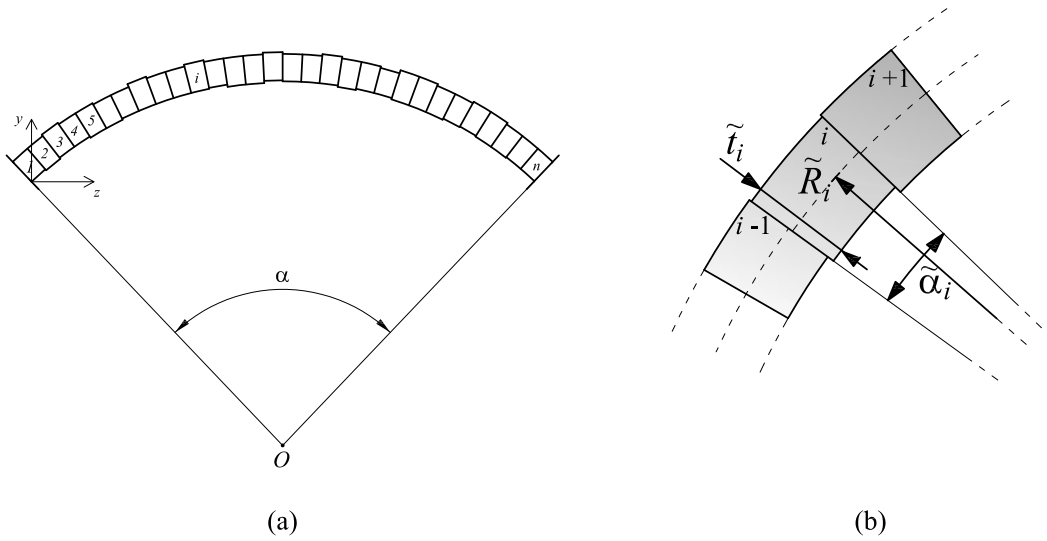

(a) (b)

Figure 5: Generic uncertain geometry of the circular arch (a) and random geometrical parameters related to the ith voissoir (b).

$$\begin{cases} \alpha_i = \alpha/n \\ t_i = t \\ R_i = R \end{cases} \tag{9}$$

The uncertainties related to the voussoirs shape have been modelled by considering these parameters as random variables (Fig. 5), with uniform probability density functions (Fig. 6). The use of a uniform probability density function defined in a specific interval is related to the concept of tolerance, as will be discussed in the following. Moreover, this assumption has allowed to avoid the definition of further parameters (such as standard deviation, etc.) and, at the same time, the possibility to obtain negative samples, as in the case of normal probability density function. The amplitude of the range of variability depends on the tolerance ε:

$$\begin{cases} \tilde{\alpha}_i = E[\tilde{\alpha}_i] + \varepsilon\ \alpha/n\ \cdot\ \tilde{p}_{\alpha_i} = \alpha/n + \varepsilon\ \alpha/n\ \cdot\ \tilde{p}_{\alpha_i} = \alpha/n\,(1 + \varepsilon\,\tilde{p}_{\alpha_i}) \\ \tilde{t}_i = E[\tilde{t}_i] + \varepsilon\ t\ \cdot\ \tilde{p}_{t_i} = t + \varepsilon\ t\ \cdot\ \tilde{p}_{t_i} = t\,(1 + \varepsilon\,\tilde{p}_{t_i}) \\ \tilde{R}_i = E[\tilde{R}_i] + \chi\ R \cdot\ \tilde{p}_{R_i} = R + \chi\ R \cdot\ \tilde{p}_{R_i} = R\,(1 + \chi\,\tilde{p}_{R_i}) \end{cases} \tag{10}$$

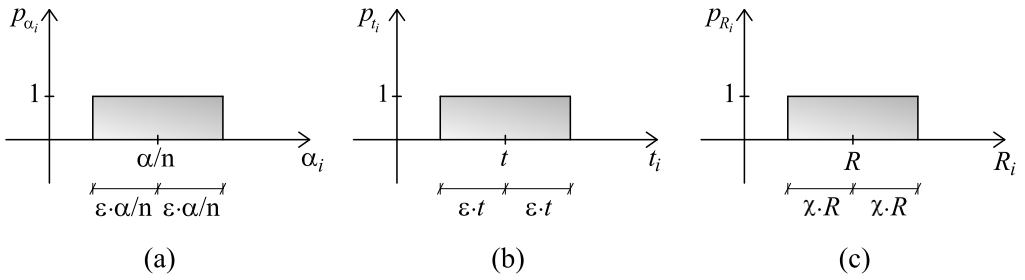

Figure 6: Probability density functions for the angle of embrace α_i (a), the thickness t_i (b) and the radius R_i (c).

where $\chi = \varepsilon \, \frac{t}{R}$ and $\tilde{p}_{\alpha_i}$, $\tilde{p}_{t_i}$, $\tilde{p}_{R_i}$ are independent samples taken from a uniform probability density function defined in the range $[-1, 1]$. The mean values of the random geometrical parameters have been assumed equal to the corresponding nominal values. The uncertain geometry has been generated by extracting n samples both for the radius $\tilde{R}_i$ and the thickness $\tilde{t}_i$. On the other hand, in order to make the angle of embrace of the arch α constant, as prescribed by the hypothesis number *ii*) at §2.5, only $n - 1$ samples of the variable $\tilde{\alpha}_i$ have been extracted for each uncertain geometry. The value of the nth angle of embrace has been determined by difference:

$$\tilde{\alpha}_n = \alpha - \sum_{i=1}^{n-1} \tilde{\alpha}_i \tag{11}$$

and then it has been checked that this value belongs to the range of definition of the random variable:

$$\alpha/n(1-\varepsilon) \, \leq \, \tilde{\alpha}_n \, \leq \, \alpha/n(1+\varepsilon) \tag{12}$$

Starting from the nominal arch described at §2.5, three different levels of geometrical uncertainty have been analysed, assuming the tolerance ε equal to 0.03, 0.05 and 0.10 and $\chi = \varepsilon \, \frac{t}{R}$ equal to 0.0045, 0.0075 and 0.015. The assumption of $\varepsilon = 0.03$ refers to the tolerance prescribed by the standard codes of the industrial, hence modern, fabrication of blocks for masonry constructions (brick masonry, stone masonry,...). The other values have been assumed to simulate effective voussoirs and/or degradation process of

the structure, analysing more suitable conditions for historical constructions.

For an assigned deterministic geometry, considering the symmetry of the structure respect to the vertical axis passing through the crown, a unique value of the nominal horizontal loads multiplier can be found. On the contrary, when an uncertain geometry is assigned, two values of the random horizontal loads multiplier $\tilde{k}_l$ and $\tilde{k}_r$ have to be determined, corresponding respectively to the direction of loads acting from left to right and from right to left. Hence, the random horizontal loads multiplier has been determined as the minimum value:

$$\tilde{k} = \min(\tilde{k}_l,\, \tilde{k}_r) \tag{13}$$

It should be noted that the adoption of an uncertain geometry implies that the transmission of the stresses between two adjacent voussoirs does not occur through the entire thickness of each voussoir anymore, but a geometrical parameter that quantifies the effective contact length $\tilde{t}^c$ along each joint has to be defined, depending on the random thickness $\tilde{t}$ and radius $\tilde{R}$ of the delimiting voussoirs:

$$\begin{cases} \tilde{t}_j^c = \tilde{t}_j & \text{for } j = 1 \\ \tilde{t}_j^c = \min(\tilde{R}_{j-1} + \frac{\tilde{t}_{j-1}}{2}, \tilde{R}_j + \frac{\tilde{t}_j}{2}) - \max(\tilde{R}_{j-1} - \frac{\tilde{t}_{j-1}}{2}, \tilde{R}_j - \frac{\tilde{t}_j}{2}) & \text{for } j = 2 \text{ to } n \\ \tilde{t}_j^c = \tilde{t}_{j-1} & \text{for } j = n+1 \end{cases} \tag{14}$$

while in deterministic conditions it results $\tilde{t}_j^c = t$ for $j = 1$ to $n+1$. Hence, the resistance criterion of Eq. (6) has necessarily to be modified, since the thrust line must be included inside the irregular boundaries of the arch, i.e. must pass through the contact length of each joint:

$$-\frac{t_j^c}{2} \leq e_j \leq \frac{t_j^c}{2} \tag{15}$$

where $j = 1$ to $n + 1$.

In the following, the effect of uncertainties on the horizontal load multiplier has been analysed by considering both the single contributions of the three random parameters and the sets of their combinations. The probabilistic approach is essentially based on the Monte Carlo method: for each set of analysis n samples have been generated by using the probability density functions previously introduced and the related distributions of the horizontal loads multiplier have been obtained. It should be noted that the limit

analysis procedure requires only a few seconds of computational cost to give the results related to each random arch.

3.2. Random angles of embrace

The effect of the random value of the angle of embrace $\tilde{\alpha}_i$ of each voussoir on the horizontal loads multiplier has been evaluated in this section. The radius R_i and the thickness t_i related to each voussoir are assumed to be deterministic variables:

$$\begin{cases} \tilde{\alpha}_i = \alpha/n\,(1+\varepsilon\tilde{p}_{\alpha_i}) \\ \tilde{t}_i = t_i = t \\ \tilde{R}_i = R_i = R \end{cases} \tag{16}$$

where $i = 1$ to n. The contact length at each joint is equal to $\tilde{t}_j^c = t$ for $j = 1$ to $n+1$, since the thickness has been considered in this section with its nominal value. A partition of the angle of embrace α of the entire arch has been generated through n random angles of embrace $\tilde{\alpha}_i$. The limit analysis has been carried out on a wide range of number of voussoirs, adopting $n = 3 \div 50$ or equivalently $1/\eta = n/\alpha = 1.1 \div 18.2$. A random horizontal loads multiplier $\tilde{k}_\eta$ corresponds to each assumed random discretization. Let us consider the set $(\tilde{\alpha}_i)_\eta$, corresponding to a discretization with $n = \alpha/\eta$ voussoirs. The set, made of n samples, has been taken from the uniform distribution of Fig. 6(a), according to Equations (11) and (12). The analysis has been carried out through the procedure described at §2.4, by varying the stereometry parameter η, for a total number of cases equal to 1000. For each sample $(\tilde{\alpha}_i)_\eta^h \in (\tilde{\alpha}_i)_\eta$, with $h = 1 \div 1000$, the random load multiplier $\tilde{k}_\eta^h \in \tilde{k}_\eta$ has been evaluated. The results of the analysis in terms of random horizontal loads multiplier have been represented in Fig. 7 by red dots, depending on the stereometry parameter. The continuous black line represents the curve obtained by linking the mean values $E[\tilde{k}_\eta]$ and the continuous green lines represent those obtained by linking the values $E[\tilde{k}_\eta] \pm \sigma[\tilde{k}_\eta]$, being σ the standard deviation. By comparing Fig. 7(a), (b), (c) and considering a fixed value of the stereometry parameter, it can be observed an increment of the variability of the horizontal loads multiplier $\tilde{k}_\eta$ when the tolerance ε increases, i.e. when the level of the geometrical uncertainty grows up.

A limit value of the stereometry parameter η_L can be defined for the analysed arch, such that the difference between the horizontal loads multiplier coming from a discretized solution and the nominal multiplier is negligible. In

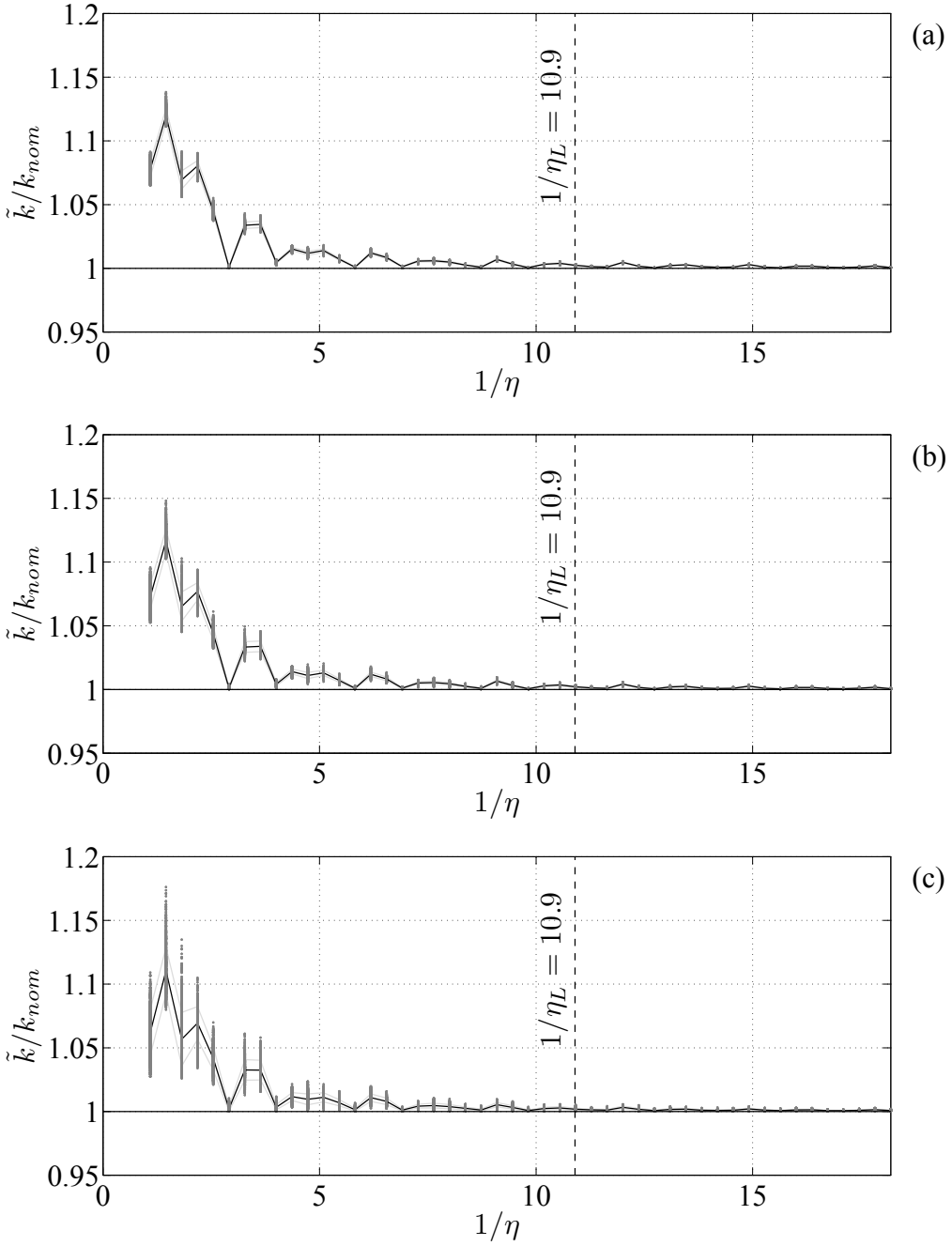

Figure 7: Horizontal loads multipliers $\tilde{k}_\eta$ (red dots) with the corresponding values $E[\tilde{k}_\eta]$ (black line) and $E[\tilde{k}_\eta] \pm \sigma[\tilde{k}_\eta]$ (green lines) for random radial discretization, depending on the stereometry parameter. Case (a) $\varepsilon = 0.03$, (b) $\varepsilon = 0.05$ and (c) $\varepsilon = 0.10$.

the following a value of $n_L = 30$ voussoirs, corresponding to $1/\eta_L = n_L/\alpha = 10.9$, has been considered, in order to have an error $(\tilde{k}_\eta - k_{nom})/k_{nom} < 1.0\%$ for each cases. Two regions can be identified in each graph: for values $1/\eta \geq 1/\eta_L$ the effect of the random angle of embrace $\tilde{\alpha}_i$ on the horizontal loads multiplier can be neglected, while in the range $1/\eta < 1/\eta_L$ the random variability of this parameter should be taken into account. In particular, it results $(\tilde{k}_\eta - k_{nom}) \to 0$ for $1/\eta \to \infty$. The explanation lies in the fact that the angle of embrace of each voussoir, deterministic or random, might determine a position of the hinges close to that of the continuous case, making the collapse multipliers coincident. In Fig. 8 the results of the analysis in terms of position of the four collapse hinges have been represented. The random values of the progressive angles $\tilde{\beta}_j$, with $j = A$, B, C, D, tends to the corresponding nominal values β_j for $1/\eta \to \infty$ (Tab. 2.5). By comparing Figures 7 and 8, it can be observed that the value of the horizontal loads multiplier is mainly determined by the position of the hinges, in particular by the hinge B. In fact, while the stereometry parameter increases, the convergence to the nominal value k_{nom} is periodically obtained when the position of the hinge B is very close to its nominal value. By referring to Fig. 7 it can be observed that the probabilistic distribution of the random horizontal loads multiplier $\tilde{k}_\eta$ is defined in a range $[\tilde{k}_\eta^{inf}, \tilde{k}_\eta^{sup}]$. In other words, the random horizontal loads multiplier is limited:

$$k_{nom} \leq \tilde{k}_\eta^{inf} \leq \tilde{k}_\eta^{h} \leq \tilde{k}_\eta^{sup} \tag{17}$$

The condition $\tilde{k}_n^{inf} = k_{nom}$ exists because in general it is possible to identify a sequence of random angles of embrace $\tilde{\alpha}_i$ corresponding to a sample $(\tilde{\alpha}_i)_\eta^h$ that produces a configuration of the collapse hinges equal to that of the continuous case. From Eq. (17) it results

$$k_{nom} \leq \tilde{k}_\eta \tag{18}$$

namely the uncertainty of the arch geometry in term of angle of embrace of each voussoir can not be associated with an horizontal loads multiplier lower than the nominal one, obtained through a continuous modelling. Eq. (18) represents the general case of Eq. (7), since the partition $(\alpha_i)_\eta$ of deterministic equal angles $\alpha_i = \alpha_{i+1}$, with $i = 1$ to $n - 1$, is a particular sample taken from the set $(\tilde{\alpha}_i)_\eta$. It can be stated that k_{nom} is the lower bound of the horizontal loads multipliers corresponding to any radial discretization, both deterministic or random. In other words, starting from a discretization of the

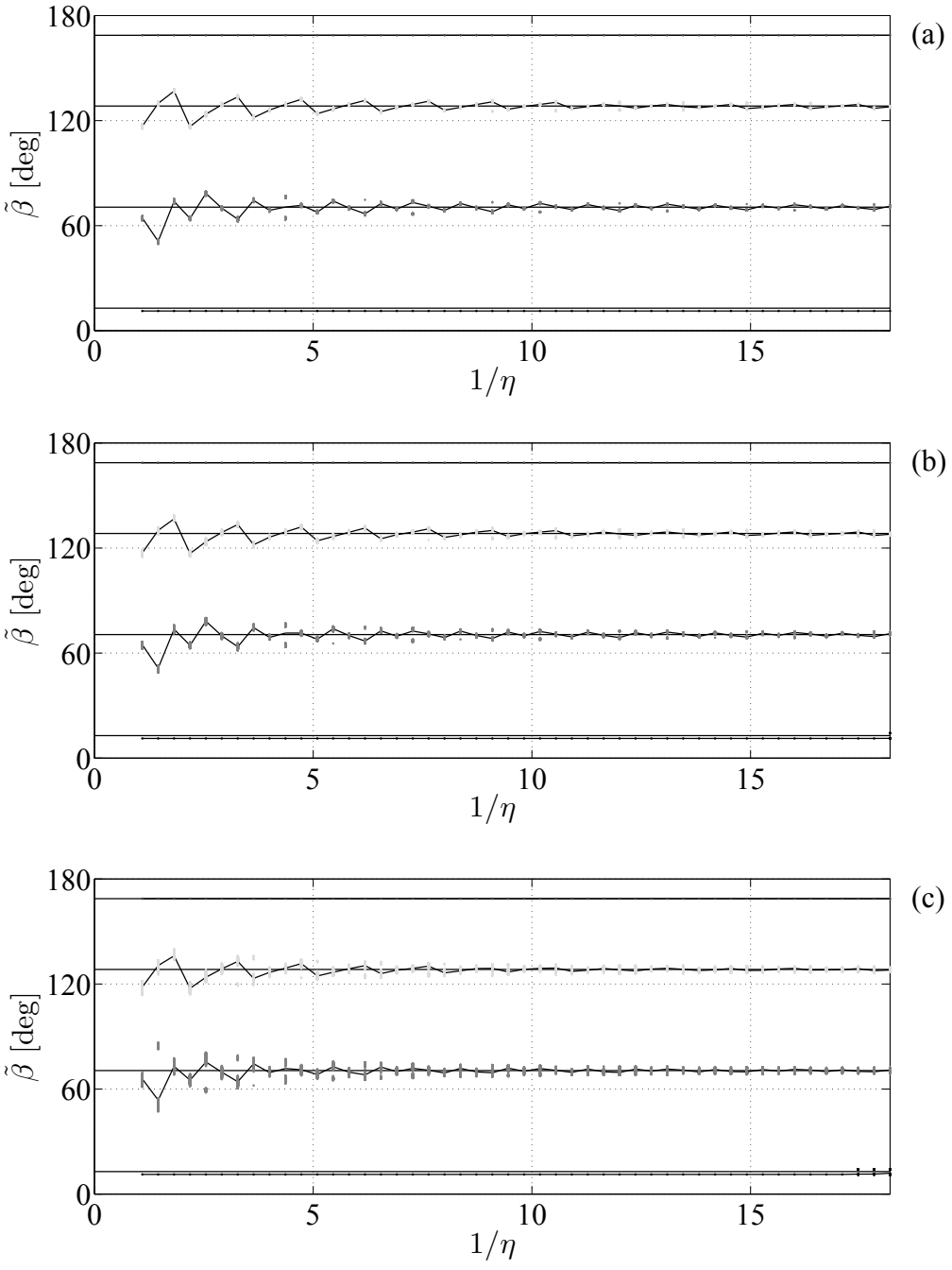

Figure 8: Position of the collapse hinges A (black), B (red), C (green), D (blue) for random radial discretization, depending on the stereometry parameter. Nominal values of progressive angles: $\beta_A = 0.2238\,\text{rad} = 12.82°$; $\beta_B = 1.2318\,\text{rad} = 70.58°$; $\beta_C = 2.2397\,\text{rad} = 128.32°$; $\beta_D = 2.9452\,\text{rad} = 168.75°$. Case (a) $\varepsilon = 0.03$, (b) $\varepsilon = 0.05$ and (c) $\varepsilon = 0.10$.

arch, modelling only its random radial stereotomy, it is not possible to find an horizontal loads multiplier inferior to that corresponding to a continuous analysis. Hence, both the continuous analysis and the analysis with a high discretization, by using $1/\eta \to \infty$ or $n \to \infty$, are on the safe side.

3.3. Range of high values of the stereometry parameter

The results of the previous paragraph §3.2 permit to state that for high values of the number of voussoirs, namely for low values of the stereometry parameter, the radial discretization of the arch is functional to the evaluation of the horizontal loads multiplier and may not necessarily represents the effective radial stereotomy, even if for arch with high values of the span length and a high number of real voussoirs there might be also a physical correspondence. In this section, the variability of the horizontal loads multiplier in the range $1/\eta \geq 1/\eta_L$ has been analysed. In particular, values of the number of voussoirs $n = 30 \div 210$ have been adopted, corresponding to $1/\eta = n/\alpha = 10.9 \div 76.4$. The analysis has been carried out step by step: in the first part only the thickness t_i has been considered as a random variable (Fig. 9(a)), while in the second part both the uncertainties due to the thickness t_i and the radius R_i have been taken into account (Fig. 9(b)). In both cases the contact length at each joint has been determined through Eq. (14). Both the analyses are necessary in order to understand the influence of each geometrical parameter on the horizontal bearing capacity of the arch. However, if these two cases are compared, it should be noted that when the radius of the voussoir is modified, even if the thickness remains the same, there is a small variation of the area and the centre of mass, i.e. of the forces and their application point, of the voussoir itself.

3.3.1. Random thickness

Since the random value of the angle of embrace of each voussoir $\tilde{\alpha}_i$ does not affect, in the considered range of $1/\eta$, the value of the horizontal loads multiplier $\tilde{k}$, the following assumption have been used in order to study the effects due to a random variation of the thickness of the voussoirs:

$$\begin{cases} \tilde{\alpha}_i = \alpha_i = \alpha/n \\ \tilde{t}_i = t\,(1 + \varepsilon \tilde{p}_{t_i}) \\ \tilde{R}_i = R_i = R \end{cases} \tag{19}$$

The uniform probability density function of Fig. 6(b) has been used for the thickness. It should be noted that the geometry, represented in Fig. 9(a),

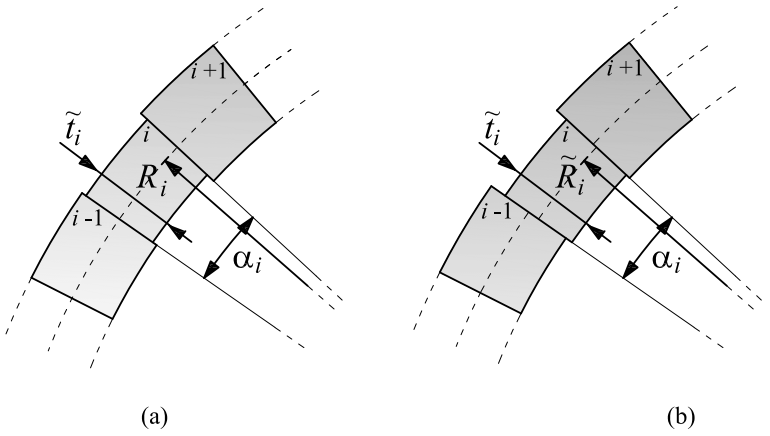

Figure 9: Uncertain geometry of the voussoirs for the case of (a) random thickness $\tilde{t}_i$ and (b) random thickness $\tilde{t}_i$ and radius $\tilde{R}_i$.

is characterized by the centroids of each joint that are placed on the mean circular construction line of the arch, since the radius R_i has been assumed as a deterministic parameter. In this case, the uncertain geometry has been generated by extracting a sample of n values of thickness $\tilde{t}_i$ for the voussoirs. Eq. (14) that defines the contact length $\tilde{t}^c$ can be written as follows:

$$\begin{cases} \tilde{t}^c_j = \tilde{t}_j & \text{for } j = 1 \\ \tilde{t}^c_j = \min\left(\frac{\tilde{t}_{j-1}}{2}, \frac{\tilde{t}_j}{2} \right) & \text{for } j = 2 \text{ to } n \\ \tilde{t}^c_j = \tilde{t}_{j-1} & \text{for } j = n+1 \end{cases} \tag{20}$$

For each of considerated cases of the stereometry parameter $1/\eta$ (in the range $1/\eta = 10.9 \div 76.4$, or equivalently $n = 30 \div 210$), the analysis has been carried out for a total number of samples equal to 1000. In this paper, only the results related to n equal to 30, 90, 150, 210 will be shown. For each set $(\tilde{t}_i)^h_\eta$ taken from the uniform probability density function of Fig. 6(b), being $n = \alpha/\eta$, the corresponding value of the random horizontal loads multiplier $\tilde{k}^h_\eta$ has been evaluated, with $h = 1 \div 1000$.

As previously asserted, the direction of the horizontal ground motion does not have any influence on the horizontal load multiplier in deterministic condition, because of the symmetry respect to the vertical axis passing though the crown, while in presence of the geometrical uncertainties two multipliers $\tilde{k}_l$ and $\tilde{k}_r$ can be defined. At each iteration h two values of horizontal loads

multiplier $\tilde{k}_l^h$ and $\tilde{k}_r^h$ have been determined in order to apply Eq. (13) and find the minimum value between them, that is the proper horizontal loads multiplier $\tilde{k}^h$. In Fig. 10 the histogram of the probability density of the horizontal loads multiplier $\tilde{k}$ has been represented, for values of n equal to 30, 90, 150, 210 and for $\varepsilon = 0.10$. The normal probability density function $p_{\tilde{k}_\eta}$ has been used in first approximation to interpolate the numerical results:

$$p_{\tilde{k}_\eta} = f(\,\tilde{k}_\eta \,|\, \mu, \sigma\,) = \frac{1}{\sigma\sqrt{2\pi}}\, e^{\frac{-(\tilde{k}_\eta - \mu)^2}{2\sigma^2}} \tag{21}$$

where $\mu = E[\tilde{k}_\eta]$ and $\sigma^2 = \sigma^2[\tilde{k}_\eta] = E[\tilde{k}_\eta - \mu]^2$ are the mean value and the variance of the sample of the random horizontal loads multipliers, with a discretization of the arch by means of $n = \alpha/\eta$ voussoirs. The histogram of the probability density of $\tilde{k}$ of Fig. 10 has been represented with its interpolant normal probability density function (continuous black line), superimposed to the interpolant normal probability density functions of $\tilde{k}_l$ (dashed black line) and $\tilde{k}_r$ (dash-dot black line). It can be observed the coincidence of the mean values $E[\tilde{k}_l] \simeq E[\tilde{k}_r]$ and of the standard deviations $\sigma[\tilde{k}_l] \simeq \sigma[\tilde{k}_r]$. Moreover it results $E[\tilde{k}] < E[\tilde{k}_l] \simeq E[\tilde{k}_r]$ and $\sigma[\tilde{k}] < \sigma[\tilde{k}_l] \simeq \sigma[\tilde{k}_r]$, namely the horizontal loads multiplier has a mean value and a standard deviation that are lower than those of $\tilde{k}_l$ and $\tilde{k}_r$. The absence of correlation between $\tilde{k}_l$ and $\tilde{k}_r$ is proved by means of the graph of Fig. 11, in which the differences $\tilde{k}_l - E[\tilde{k}_l]$ have been plotted versus the differences $\tilde{k}_r - E[\tilde{k}_r]$. The increment of dispersion of the results appears if the number of voussoirs increases.

In Fig. 12 the results related to the random horizontal loads multiplier have been represented by red dots, depending on $1/\eta$. The interpolating normal probability density has been plotted for each set $\tilde{k}_\eta$. The black line links the mean values $E[\tilde{k}_\eta]$ and shows a decreasing trend when $1/\eta$ increases. The standard deviation $\sigma[\tilde{k}_\eta]$ also decreases when $1/\eta$ increases. The green line corresponds to the horizontal loads multiplier $k_{nom}(\alpha, t_{min}, R)$ obtained from a deterministic arch having a radius R, an angle of embrace α and a thickness $t_{min} = t(1-\varepsilon)$ equal to the minimum value of the definition range of its probability density function (Fig. 6(b)). The value $k_{nom}(\alpha, t_{min}, R)$ could be thought as the lower bound of the horizontal loads multiplier for this type of uncertain geometry. Actually, it results:

$$k_{nom}(\alpha, t_{min}, R) < E[\tilde{k}_\eta] \tag{22}$$

The mean value of the random horizontal loads multiplier $E[\tilde{k}_\eta]$ never

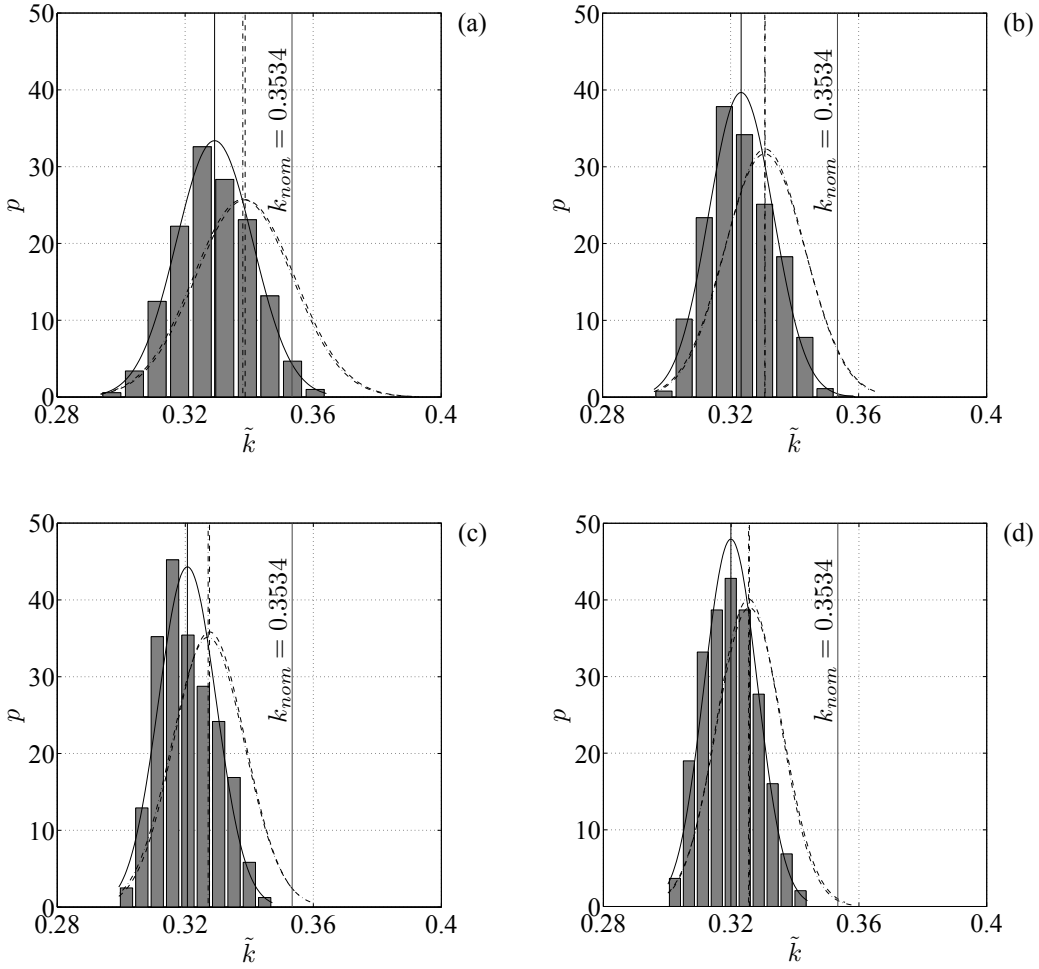

Figure 10: Histogram of the probability density of the horizontal loads multiplier $\tilde{k}$ with its interpolant normal probability density function (continuous black line) and with the indication of the nominal horizontal loads multiplier (blue line), superimposed to the interpolant normal probability density functions of $\tilde{k}_l$ (dashed black line) and $\tilde{k}_r$ (dash-dot black line), for $\varepsilon = 0.10$. Cases of random thickness: (a) $n = 30$, (b) $n = 90$, (c) $n = 150$, (d) $n = 210$.

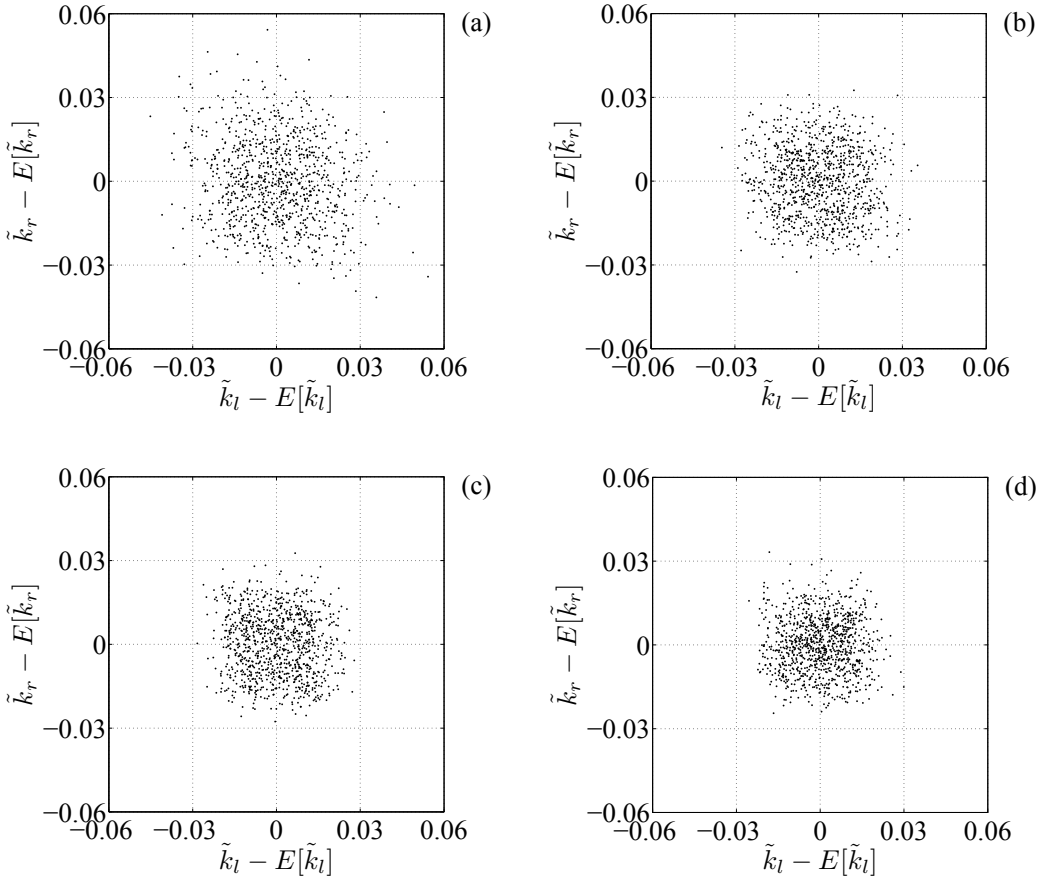

Figure 11: Correlation between the differences $\tilde{k}_l - E[\tilde{k}_l]$ and $\tilde{k}_r - E[\tilde{k}_r]$ for $\varepsilon = 0.10$. Cases of random thickness: (a) $n = 30$, (b) $n = 90$, (c) $n = 150$, (d) $n = 210$.

reaches $k_{nom}(\alpha, t_{min}, R)$, but tends to a greater value. The motivation lies in the fact that the combination of two different aspects plays a fundamental role in the definition of the value of the random horizontal loads multiplier $\tilde{k}$. From one side, the random thickness $\tilde{t}_i$ produces a reduction of $\tilde{k}$ because the resistance domain has been modified in Eq. (15) through the definition of the contact length $\tilde{t}^c$, whose mean value $E[\tilde{t}^c]$ for an assigned random geometry is lower than the nominal thickness t. On the other side, the random thickness $\tilde{t}_i$ can modify the position of the hinges respect to the nominal case, producing an increment of the value of $\tilde{k}$. Let us consider the set of results in the case of $\varepsilon = 0.10$ for $1/\eta = 10, 91$ ($n = 30$) (red dots for $1/\eta = 10, 91$ of Fig. 12(c)). In Fig. 13 the uncertain geometries corresponding to the minimum ($k = 0.294$), the intermediate ($k = 0.328$) and the maximum ($k = 0.364$) horizontal loads multiplier of this set of multipliers have been represented with the corresponding thrust lines. The horizontal loads act from left to right. It can be observed that the hinge B moved toward the left adjacent joint when passing from the condition of minimum multiplier of Fig. 13(a) to the condition of intermediate multiplier of Fig. 13(b). In the condition of maximum multiplier of Fig. 13(c) also the hinge C moved toward the left adjacent joint. The movement of the hinges is mainly dictated by the position of the voussoir that has, within the region of the nominal position of the hinges, the biggest reduction of the thickness.

A reduction of the standard deviation has been observed when n increases: the greater is the number of voussoirs, the higher is the probability to obtain a stable configuration of the hinges position. In other words, if the number of voussoirs is high, the position of the collapse hinges has a low shifting from an iteration h to the next one and the variation of the horizontal loads multiplier is low.

3.3.2. Random thickness and radius

In this section, the issue about the evaluation of the effects of the geometrical uncertainties on the collapse condition of the masonry arch has been completed in the range of high values of the number of voussoirs. In particular, both random values of the thickness $\tilde{t}_i$ and the radius $\tilde{R}_i$ have been adopted, while the angle of embrace of each voussoir $\tilde{\alpha}_i$ has been considered equal to its nominal value:

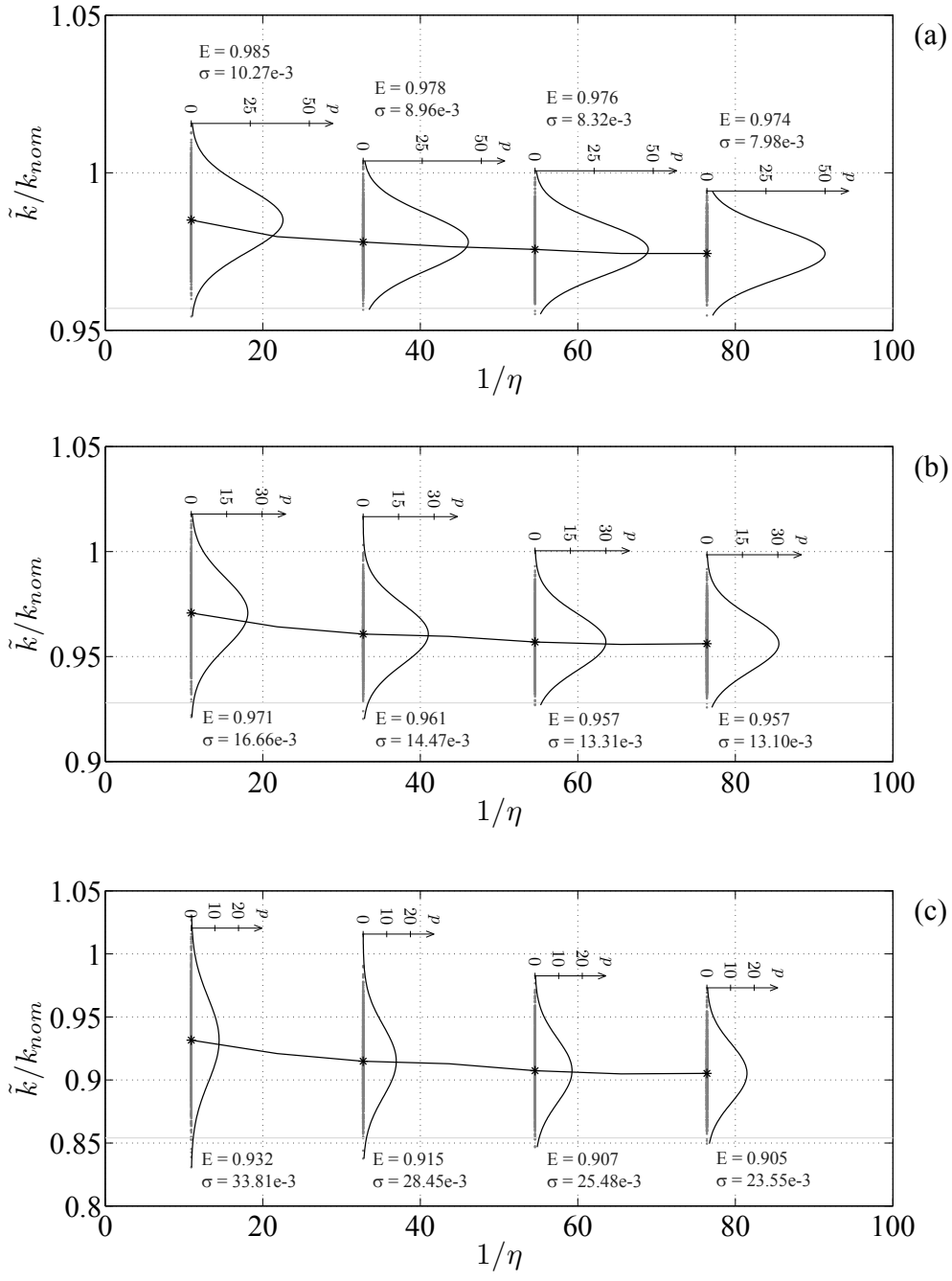

Figure 12: Horizontal loads multipliers for $n = 30$, 90, 150, 210 (red dots) compared to $k_{nom}(\alpha, t_{min}, R)$ (green line) and interpolant normal probability density function, depending on the stereometry parameter. Cases of random thickness: (a) $\varepsilon = 0.03$, (b) $\varepsilon = 0.05$ and (c) $\varepsilon = 0.10$.

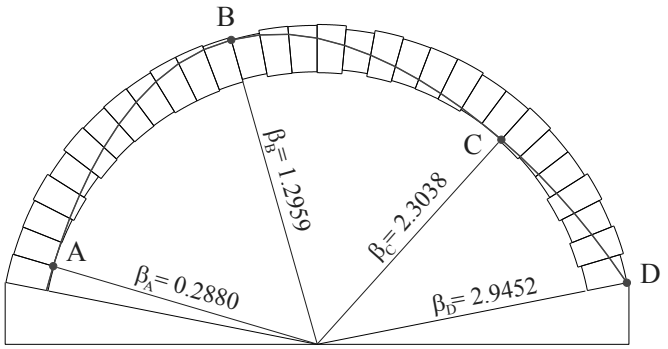

(a)

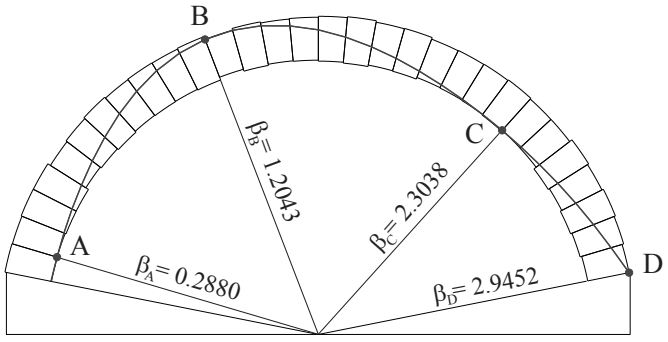

(b)

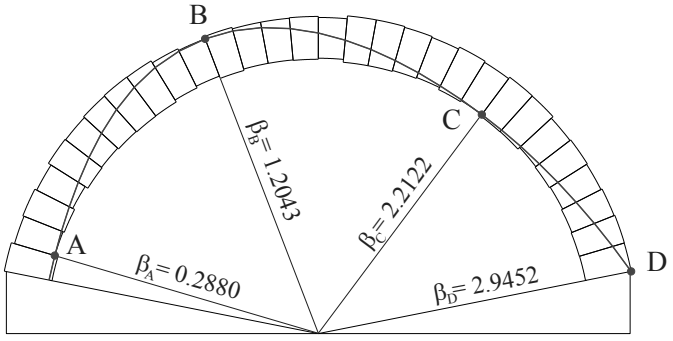

(c)

Figure 13: Examples of arches with random thickness with the corresponding thrust lines, for a number of voussoirs n equal to 30 ($1/\eta = 10, 91$) and for $\varepsilon = 0.10$. Case (a) minimum ($k = 0.294$), (b) intermediate ($k = 0.328$) and (c) maximum horizontal loads multiplier ($k = 0.364$).

$$\begin{cases} \tilde{\alpha}_i = \alpha_i = \alpha/n \\ \tilde{t}_i = t(1 + \varepsilon\, \tilde{p}_{t_i}) \\ \tilde{R}_i = R(1 + \chi \tilde{p}_{R_i}) \end{cases} \tag{23}$$

The uniform probability density functions of Fig. 6(b) and (c) have been used respectively for the thickness and the radius. The contact length $\tilde{t}^c$ can be evaluated by means of Eq. (14). The resulting uncertain geometry depicted in Fig. 9(b) may reproduce, in a probabilistic sense, a more realistic condition of the arch geometry in the field of high values of n – since it has been already proved that a deterministic value of α_i can be adopted in this range.

As well as in §3.3.1, the analysis has been carried out for a number of cases equal to 1000 by varying the stereometry parameter η. A sample of n values of thickness $\tilde{t}_i$ and a sample of n values of radius $\tilde{R}_i$ have been independently extracted at each case. For each couple of sets $(\tilde{t}_i)^h_\eta$ and $(\tilde{R}_i)^h_\eta$ being $n = \alpha/\eta$, the corresponding value of the random horizontal loads multiplier $\tilde{k}^h_\eta$ has been evaluated.

The analysis has been carried out all over the range $n = 30 \div 210$, corresponding to $1/\eta = n/\alpha = 10.9 \div 76.4$, but the results will be shown only for certain values of the number of voussoirs n equal to 30, 90, 150, 210. In Fig. 14 the histogram of the probability density of the horizontal loads multiplier $\tilde{k}$ has been represented for $\varepsilon = 0.10$ with its interpolant normal probability density function (continuous black line), superimposed to the interpolant normal probability density functions of $\tilde{k}_l$ (dashed black line) and $\tilde{k}_r$ (dash-dot black line), in comparison to the nominal multiplier k_{nom} (blue vertical line). It can be observed again as the mean values and of the standard deviations of the random variables $\tilde{k}_l$ and $\tilde{k}_r$ are very close. Moreover, it results $E[\tilde{k}] < E[\tilde{k}_l] \simeq E[\tilde{k}_r]$ and $\sigma[\tilde{k}] < \sigma[\tilde{k}_l] \simeq \sigma[\tilde{k}_r]$. The absence of correlation between $\tilde{k}_l$ and $\tilde{k}_r$ is proved by means of the graphs of Fig. 15.

In Fig. 16 the results related to the random horizontal loads multiplier have been represented by red dots with the interpolant normal probability density function defined according to Eq. (21). Similar considerations to those of section §3.3.1 can be made regarding the trend of the mean values and the standard deviations of the horizontal loads multiplier $\tilde{k}_\eta$. Also in this case, the reduction of the mean value of the horizontal loads multiplier $E[\tilde{k}_\eta]$ respect to the nominal value k_{nom} is related to the further reduction of the mean value of the contact length $E[\tilde{t}^c]$ respect to the nominal thickness

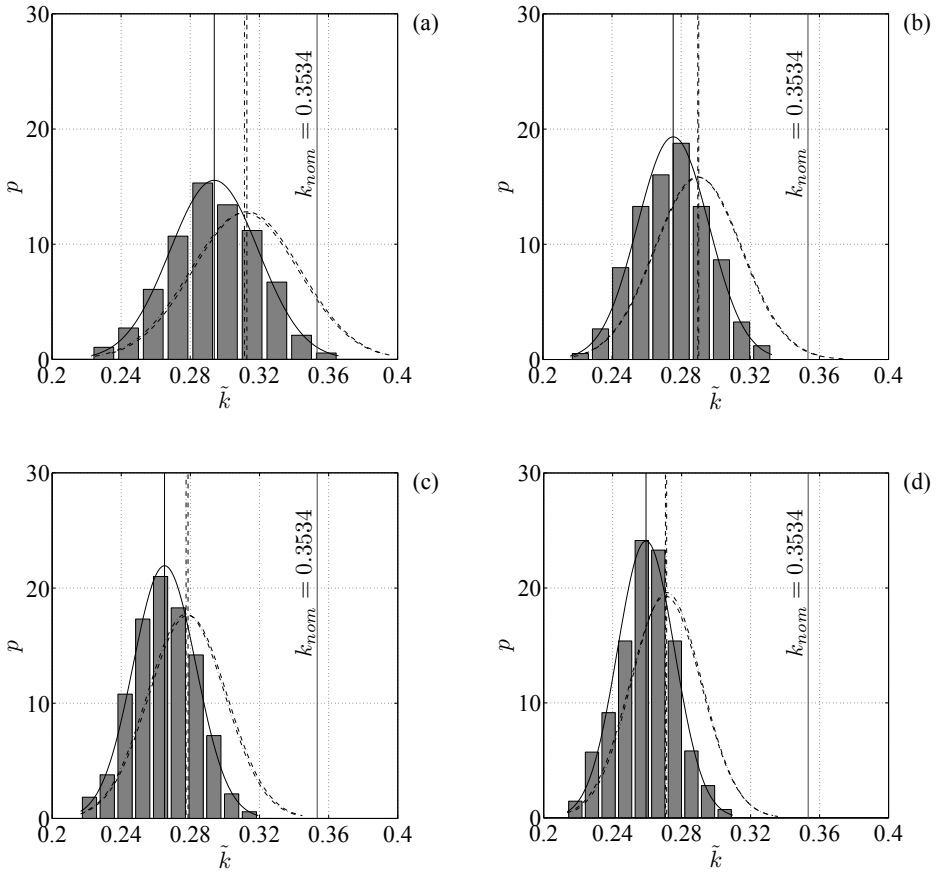

Figure 14: Histogram of the probability density of the horizontal loads multiplier $\tilde{k}$ with its interpolant normal probability density function (continuous black line) and with the indication of the nominal horizontal loads multiplier (blue line), superimposed to the interpolant normal probability density functions of $\tilde{k}_l$ (dashed black line) and $\tilde{k}_r$ (dash-dot black line), for $\varepsilon = 0.10$. Cases of random thickness and radius: (a) $n = 30$, (b) $n = 90$, (c) $n = 150$, (d) $n = 210$.

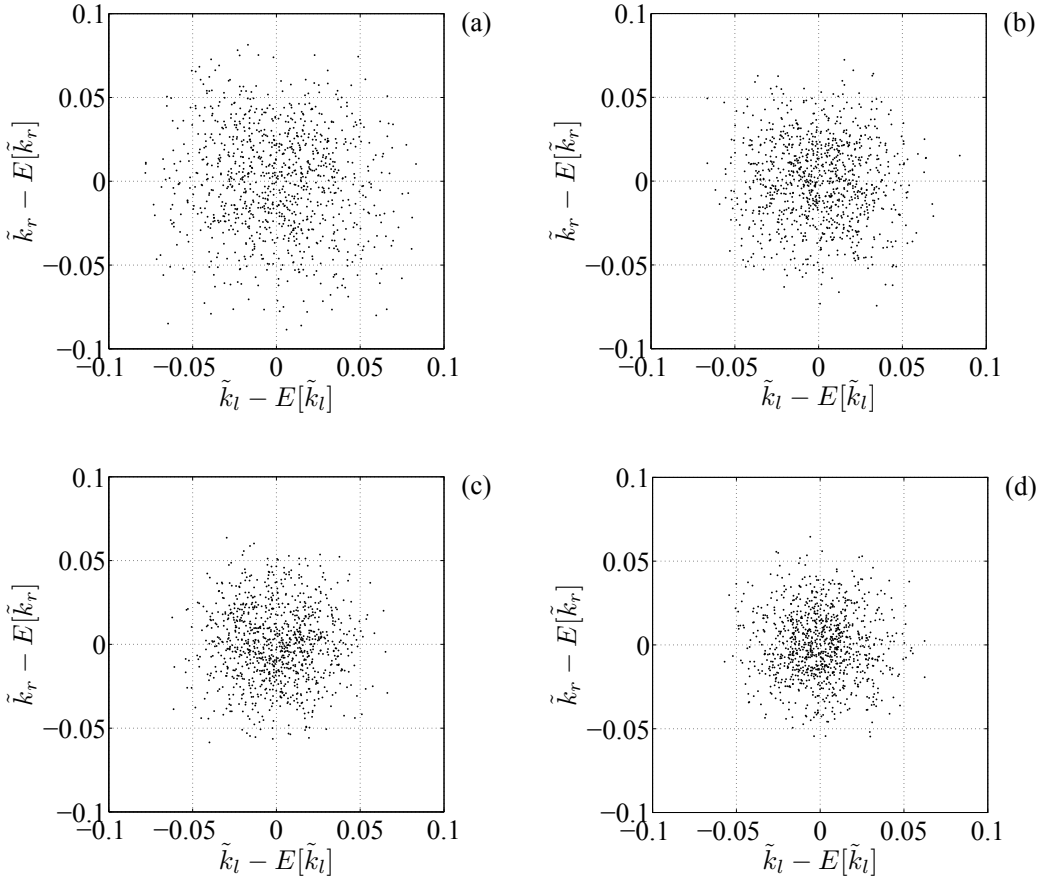

Figure 15: Correlation between the differences $\tilde{k}_l - E[\tilde{k}_l]$ and $\tilde{k}_r - E[\tilde{k}_r]$ for $\varepsilon = 0.10$. Cases of random thickness and radius: (a) $n = 30$, (b) $n = 90$, (c) $n = 150$, (d) $n = 210$.

t, due to the random radius $\tilde{R}_i$. A reduction of both the mean value $E[\tilde{k}_\eta]$ and the standard deviation $\sigma[\tilde{k}_\eta]$ of the horizontal loads multiplier has been observed if the number of voussoirs increases. From the comparison between Fig. 12 and Fig. 16, a further reduction of $\tilde{k}_\eta$ can be observed if the uncertainties on the radius are considered. The reason lies in the change of the contact lengths $\tilde{t}_j^c$. In the previous case of paragraph §3.3.1, in which the thickness t_i is the unique random variable, the law of the contact length has been defined by means of Eq. (20) and it results $t(1-\varepsilon) \leq \tilde{t}_j^c \leq t(1+\varepsilon)$. In this case, on the contrary, the contact length can be evaluated through the general Eq. (14) and it has a higher range of variability because of the random value of $\tilde{R}_i$. The blue horizontal line of Fig. 16 corresponds to the horizontal loads multiplier $k_{nom}(\alpha, t_{min}, R_{max})$ obtained from a deterministic arch having a radius $R_{max} = R(1+\chi)$ equal to the maximum value of its definition range, an angle of embrace α and a thickness $t_{min} = t(1-\varepsilon)$ equal to the minimum value of its definition range. For this type of uncertain geometry, $k_{nom}(\alpha, t_{min}, R_{max})$ could be thought as the lower bound of the horizontal loads multiplier. In fact, as known, if the angle of embrace of the arch α has been fixed, a reduction of the horizontal loads multiplier can be obtained by decreasing the thickness and increasing the radius [29]. Actually, except for values of $1/\eta$ less than about 21.8, corresponding to $n < 60$, it results:

$$k_{nom}(\alpha, t_{min}, R_{max}) > E[\tilde{k}_\eta] \tag{24}$$

being $k_{nom}(\alpha, t_{min}, R_{max}) < k_{nom}(\alpha, t_{min}, R)$. The mean value of the random horizontal loads multiplier $E[\tilde{k}_\eta]$ may be lower than the value $k_{nom}(\alpha, t_{min}, R_{max})$ because of the uncertainties on the radius combined with those of the thickness that cause a high reduction of the average contact length, as highlighted above. In Fig. 17 the uncertain geometries corresponding to the minimum ($k = 0.223$), the intermediate ($k = 0.293$) and the maximum ($k = 0.366$) horizontal loads multiplier of the set of multipliers $\tilde{k}_\eta$ of Fig. 16(c), for $\eta = 10, 91$ ($n = 30$), have been represented with the corresponding thrust lines. The hinges A, B and C moved toward a left adjacent joint when passing from the condition of minimum multiplier of Fig. 17(a) to the condition of intermediate multiplier of Fig. 17(b). In the condition of maximum multiplier of Fig. 17(c) the hinge B further moved toward left, while the hinge A moved toward a right adjacent joint.

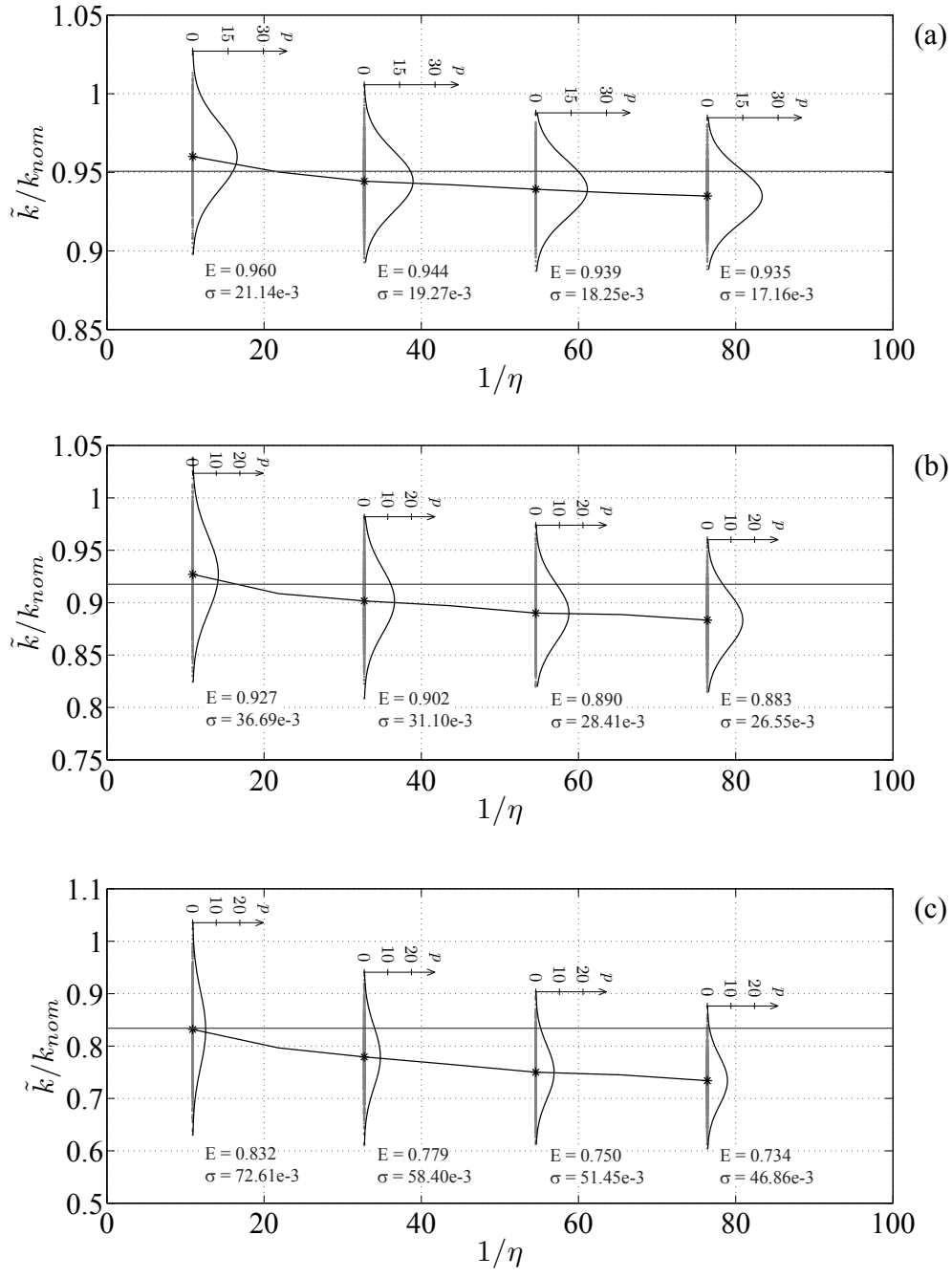

Figure 16: Horizontal loads multipliers for $n = 30, 90, 150, 210$ (red dots) compared to $k_{nom}(\alpha, t_{min}, R_{max})$ (blue line) and interpolant normal probability density function, depending on the stereometry parameter. Cases of random thickness and radius: (a) $\varepsilon = 0.03$, (b) $\varepsilon = 0.05$ and (c) $\varepsilon = 0.10$.

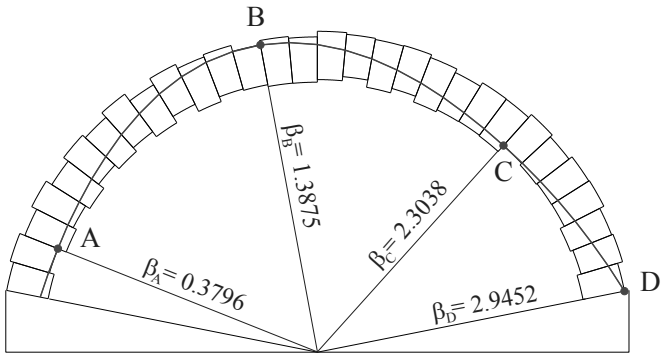

(a)

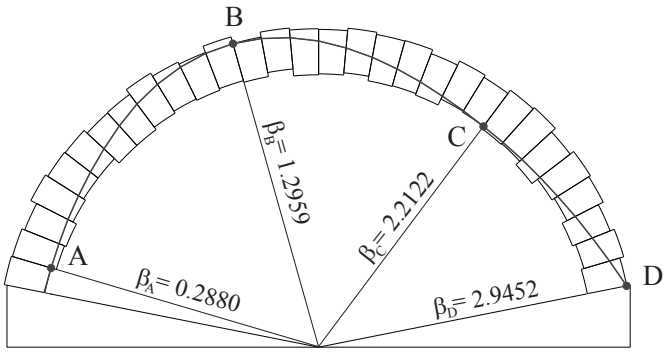

(b)

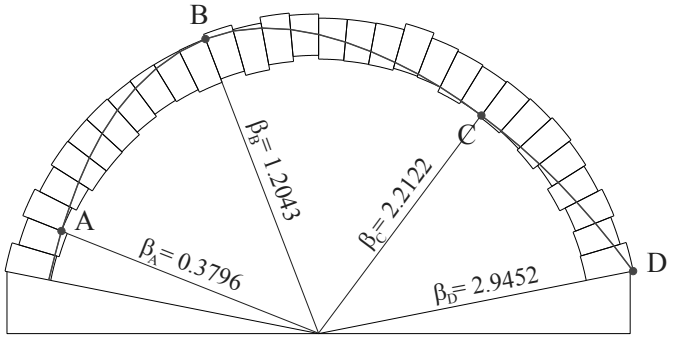

(c)

Figure 17: Examples of arches with random thickness and radius with the corresponding thrust lines, for a number of voussoirs n equal to 30 ($1/\eta = 10,91$) and for $\varepsilon = 0.10$. Case (a) minimum ($k = 0.223$), (b) intermediate ($k = 0.293$) and (c) maximum horizontal loads multiplier ($k = 0.366$).

3.4. Range of low values of the stereometry parameter: random thickness, radius and angle of embrace of the voussoirs

When modelling the arch through a discretization that uses a low value of the number of voussoirs, all the parameters involved – i.e. the thickness t_i, the radius R_i and the angle of embrace α_i – should be considered as random variables. Following the observations at §3.2 about the role played by the angle of embrace α_i, in this section the variability of the horizontal loads multiplier in the range $1/\eta < 1/\eta_L$ has been analysed. Values of the number of voussois equal to $n = 3 \div 29$ have been considered, corresponding to $1/\eta = n/\alpha = 1.1 \div 10.6$. The random values of the the angle of embrace, thickness and the radius, expressed by Eq. (10), produce the uncertain geometry depicted in Fig. 5. The contact length $\tilde{t}_j^c$ at each joint has been determined through Eq. (14). For an assigned value of η, at each case h, with $h = 1 \div 1000$, three independent sets $(t_i)_\eta^h$, $(R_i)_\eta^h$ and $(\alpha_i)_\eta^h$ of samples have been extracted from the uniform probability density functions of Fig. 6, according to Equations (11) and (12) for what concerns the angle of embrace. Then, the corresponding value of the random horizontal loads multiplier k_η^h has been evaluated. Even if all the range $n = 3 \div 29$ has been analysed, in this section only the results related to the cases $n = 5$, 10, 15, 20 will be shown.

In Fig. 18 the histogram of the probability density of the horizontal loads multiplier $\tilde{k}$ has been represented for $\varepsilon = 0.10$, with its interpolant normal probability density function (continuous black line), superimposed to the interpolant normal probability density functions of $\tilde{k}_l$ (dashed black line) and $\tilde{k}_r$ (dash-dot black line). The nominal multiplier k_{nom} has been indicated by means of a blue vertical line. It can be observed again thet the mean and the standard deviations values of the random variables $\tilde{k}_l$ and $\tilde{k}_r$ are very close. Also in this case of low values of the number of voussoirs there is no correlation between $\tilde{k}_l$ and $\tilde{k}_r$, as shown in Fig. 19.

The results in term of $\tilde{k}_\eta$ related to the cases $n = 5$, 10, 15, 20 have been represented in Fig. 20, for different values of the tolerance ε. Each value of k_η^h has been depicted by a red dot and a black line has been drawn linking the mean values $E[\tilde{k}_\eta]$. The interpolant normal probability density function, defined according to Eq. (21), has been represented at each value of η. The effect of the random value of the angle of embrace $\tilde{\alpha}_i$ immediately appears from the irregular trend of this black line, as previously observed at §3.2 with reference to Fig. 7. For very low values of $1/\eta$ the horizontal loads multiplier

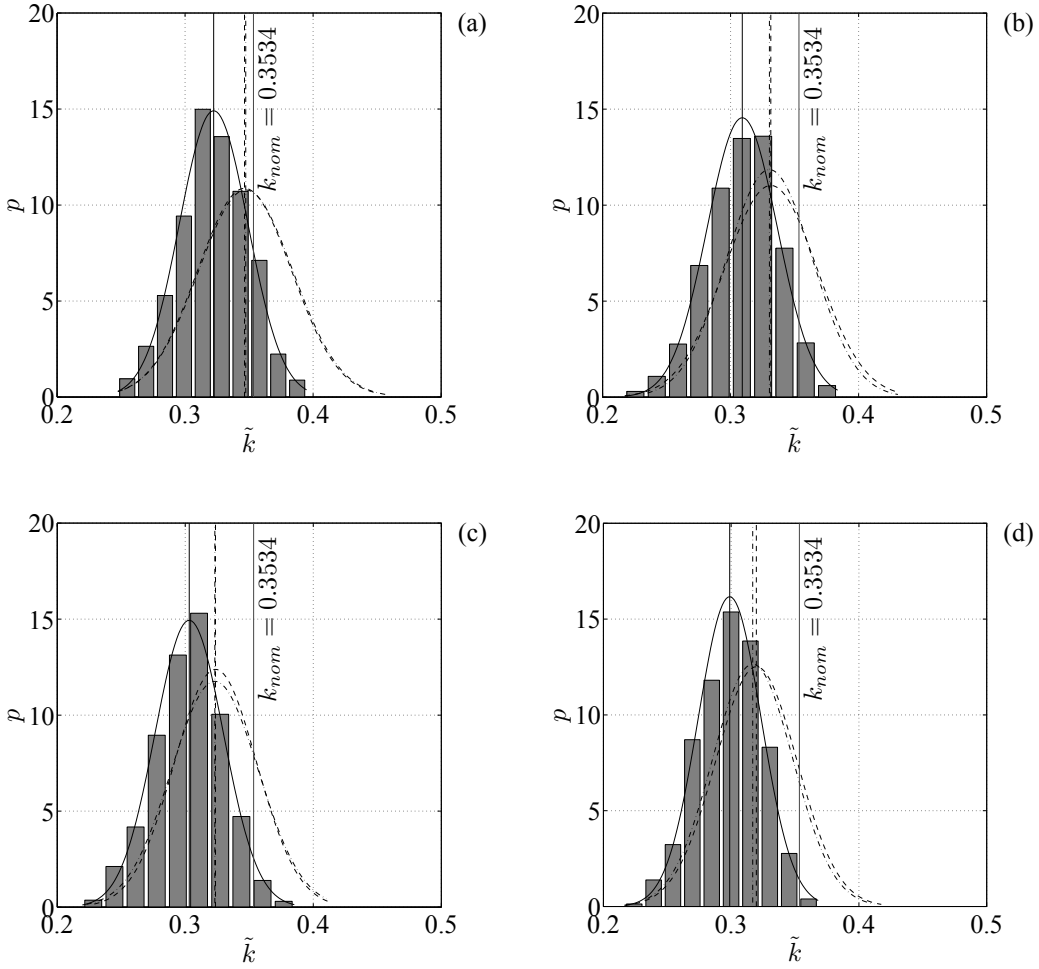

Figure 18: Histogram of the probability density of the horizontal loads multiplier $\tilde{k}$ with its interpolant normal probability density function (continuous black line) and with the indication of the nominal horizontal loads multiplier (blue line), superimposed to the interpolant normal probability density functions of $\tilde{k}_l$ (dashed black line) and $\tilde{k}_r$ (dash-dot black line), for $\varepsilon = 0.10$. Cases of random angle of embrace, thickness and radius: (a) $n = 5$, (b) $n = 10$, (c) $n = 15$, (d) $n = 20$.

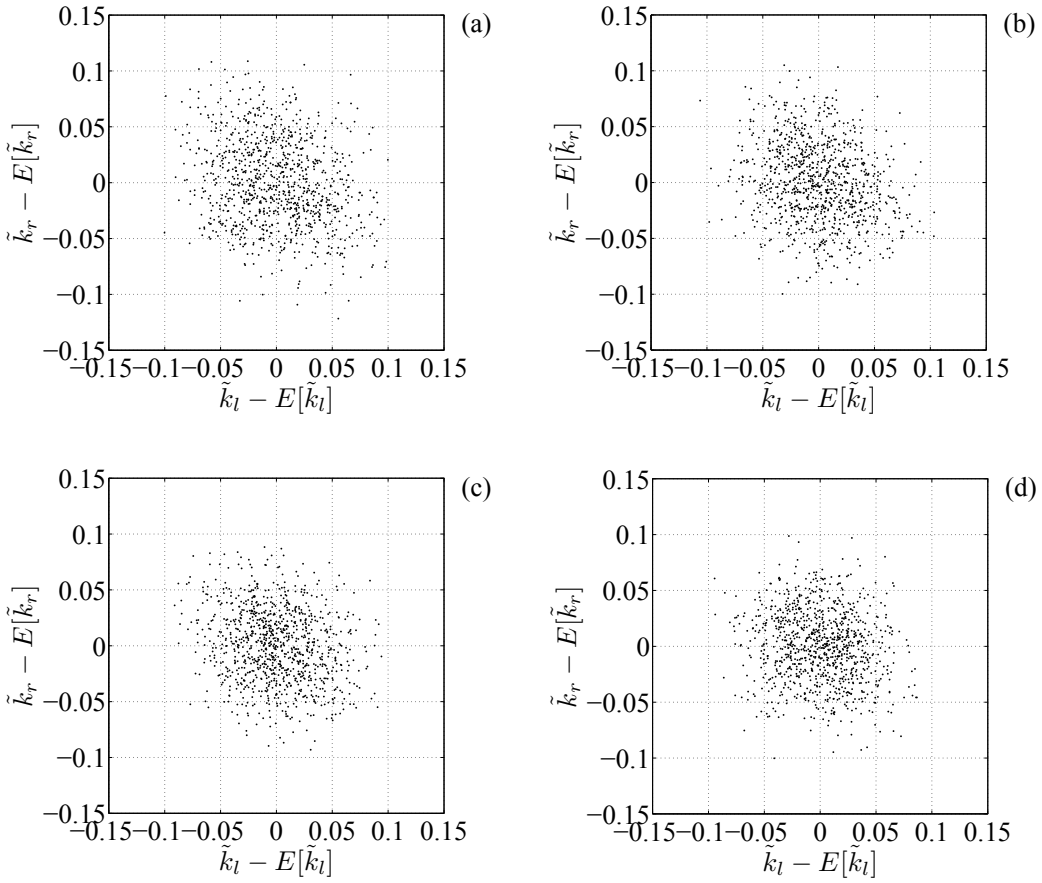

Figure 19: Correlation between the differences $\tilde{k}_l - E[\tilde{k}_l]$ and $\tilde{k}_r - E[\tilde{k}_r]$ for $\varepsilon = 0.10$. Cases of random angle of embrace, thickness and radius: (a) $n = 5$, (b) $n = 10$, (c) $n = 15$, (d) $n = 20$.

$\tilde{k}_\eta$ may be greater than the nominal multiplier, but further increasing the number of voussoirs its value decreases, reaching the condition $\tilde{k}/k_{nom} < 1$. In Fig. 21 the geometries corresponding to the minimum ($k = 0.229$), the intermediate ($k = 0.315$) and the maximum ($k = 0.399$) horizontal loads multiplier of the set $\tilde{k}_\eta$ of Fig. 20(c), for $1/\eta = 3,64$ ($n = 10$), have been represented with the corresponding thrust lines. It can be observed that when passing from the condition of minimum multiplier of Fig. 21(a) to the condition of intermediate multiplier of Fig. 21(b), the hinge A moved towards the adjacent left joint. In Fig. 21(c) the hinges B and C also moved in the same way towards left.

4. Safety factor for the nominal horizontal loads multiplier

The previous results show that, if the geometrical uncertainties are neglected, the horizontal bearing capacity might be overestimated. In order to take into account the uncertain geometry, a safety factor γ_s to be applied to the nominal multiplier in order to obtain the effective one k_e is proposed

$$k_e = \gamma_s \, k_{nom} \tag{25}$$

Given the previous results, the safety factor has been assumed equal to

$$\gamma_s = \frac{E[\tilde{k}] - \sigma[\tilde{k}]}{k_{nom}} \tag{26}$$

and it has been represented in Fig. 22 depending on the stereometry parameter η and for several values of the tolerance ε. In particular, the results related to the cases of random thickness and radius of paragraph §3.3.2 and random angle, thickness and radius of section §3.4 have been represented together, covering a range $n = 3 \div 210$ of the number of voussoirs ($1/\eta = 1.1 \div 76.4$). Each curve links the numerical factors γ_s and refers to a constant value of the tolerance ε, which can be chosen depending on the imprecisions of construction, the shape defects of the voussoirs or the deterioration level.

5. Conclusions

In this paper, a limit analysis based procedure has been developed in order to evaluate the collapse condition of the circular masonry arch with uncertain

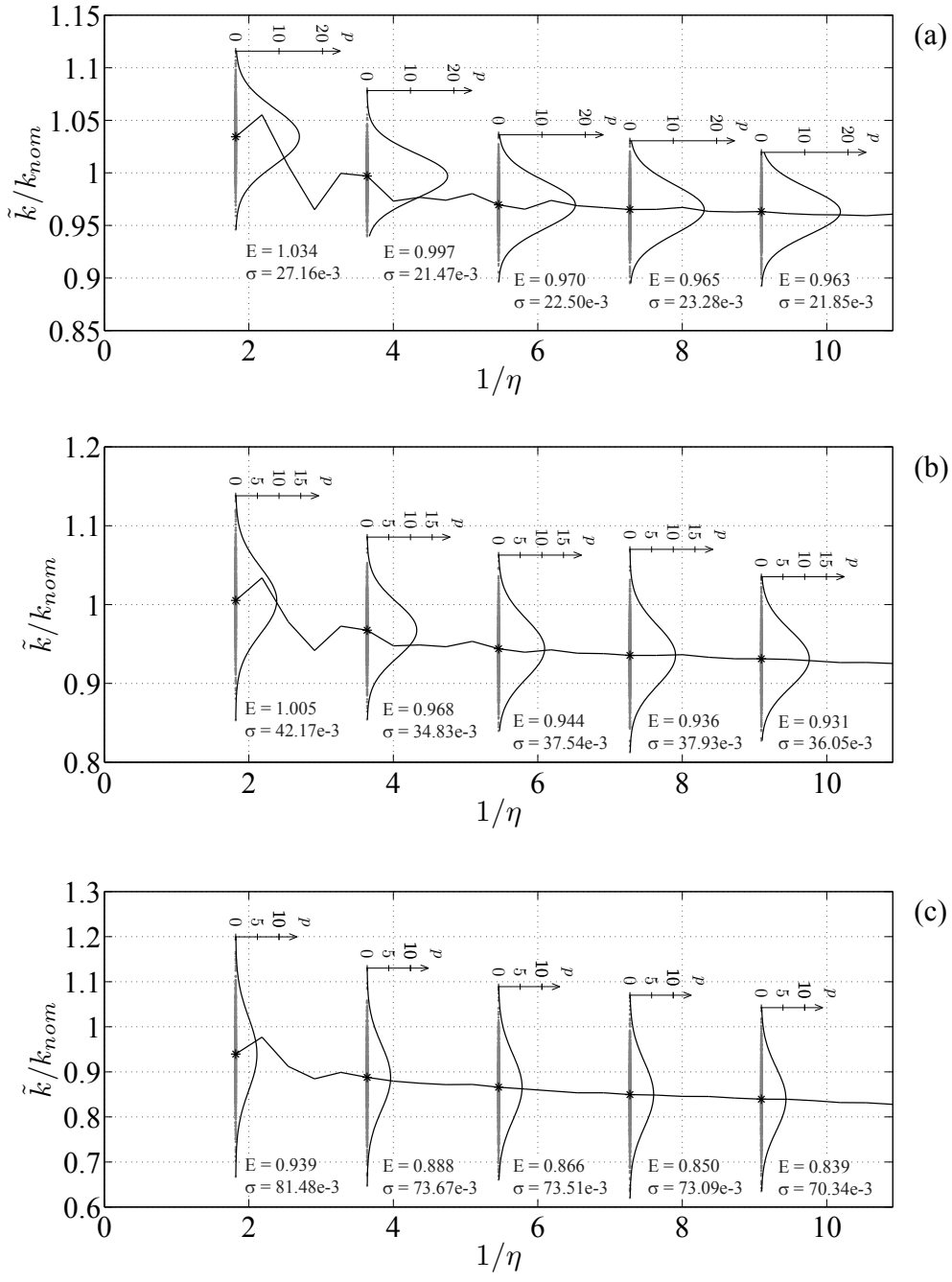

Figure 20: Horizontal loads multipliers for $n = 5, 10, 15, 20$ (red dots) and interpolant normal probability density function, depending on the stereometry parameter. Cases of random thickness and radius: (a) $\varepsilon = 0.03$, (b) $\varepsilon = 0.05$ and (c) $\varepsilon = 0.10$.

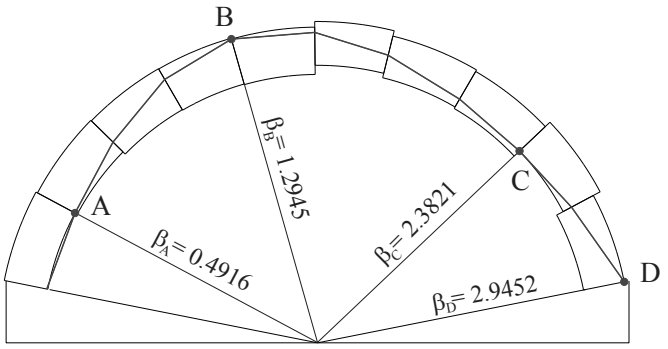

(a)

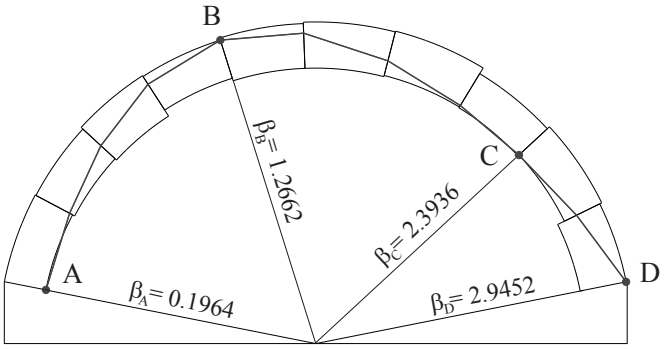

(b)

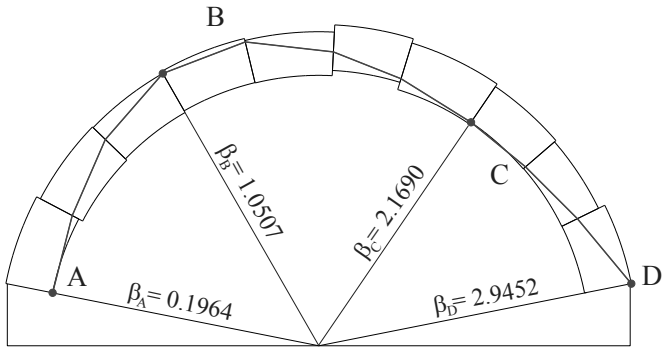

(c)

Figure 21: Examples of arches with random angle of embrace, thickness and radius with the corresponding thrust lines, for a number of voussoirs n equal to 10 ($1/\eta = 3,64$) and for $\varepsilon = 0.10$. Case (a) minimum ($k = 0.229$), (b) intermediate ($k = 0.315$) and (c) maximum horizontal loads multiplier ($k = 0.399$).

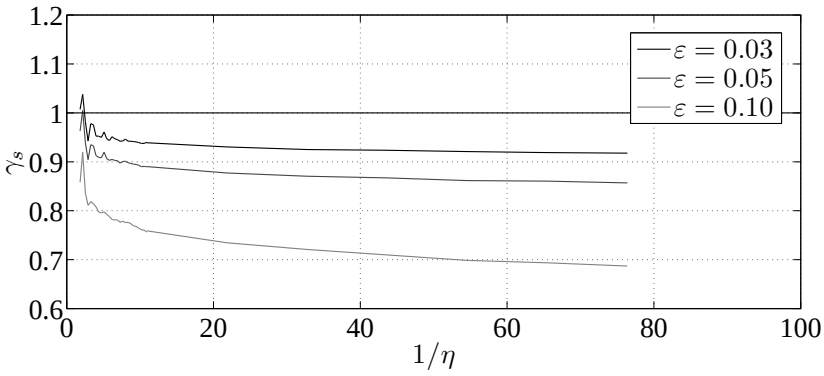

Figure 22: Safety factor γ_s of the analysed circular masonry arch with uncertain geometry, depending on the stereometry parameter.

geometry. The thickness, the radius of the mean circular construction line of the arch and the angle of embrace of each voussoir have been considered as random variables with independent uniform probability density functions.

The results have been provided in term of horizontal loads multiplier, depending on a specifically introduced stereometry parameter that is equal to the ratio between the number of voussoirs and the arch embrace angle. The results have been compared with those obtained using the nominal geometry. A limit value for the stereometry parameter has been introduced, beyond which the effect of the embrace angle randomness of the voussoirs can be neglected.

For stereometry parameters lower than the limit one, if the arch is modelled adopting deterministic values of thickness and radius but reproducing the randomness of the angle of embrace of each voussoir, an unsafe solution in term of horizontal loads multiplier may be obtained.

Viceversa, a considerable reduction of the nominal horizontal loads multiplier may result if all the geometrical uncertainties are taken into account. The value of the horizontal loads multiplier is influenced by the variation of the hinges position, due to the geometrical uncertainties, respect to the nominal condition. The shifting of the hinges is mainly dictated by the the voussoir that shows, within the region of the nominal position of the hinges, the biggest reduction of the thickness.

Finally, safety factor that should be applied to the nominal horizontal loads multiplier has been introduced in order to obtain the effective one.

Even if further studies are necessary to consider the uncertainties effect on different nominal shapes (e.g. pointed arches) and to relax the hypotheses adopted in this work (e.g. correlation between the geometrical uncertainties, not radial joints, random value of the entire arch angle of embrace, *etc.*), the obtained results are interesting to achieve more reliable seismic assessment of masonry arches.

References

[1] S. Huerta, Mechanics of masonry vaults: The equilibrium approach, in: Proceedings of Historical Constructions, Universidade do Minho, Guimaraes, Portugal, 2001, pp. 47–69.

[2] E. Benvenuto, An Introduction to the History of Structural Mechanics, Springer, Verlag, 1991.

[3] S. Timoshenko, History of Strength of Materials. Part II: Vaulted Structures and Elastic Systems, Dover Publications, Inc., 1953.

[4] J. Heyman, The safety of masonry arches, International Journal of Mechanical Sciences 11 (1969) 363–385.

[5] J. Heyman, The masonry arch, Ellis Horwood Ltd., Chinchester, 1982.

[6] M. Farshad, On optimal form of arches, Journal of the Franklin Institute 302 (1976) 187–194.

[7] G. Marano, F. Trentadue, F. Petrone, Optimal arch shape solution under static vertical loads, Acta Mechanica 225 (2014) 379–686.

[8] C. Wang, C. Wang, Closed-form solutions for funicular cables and arches, Acta Mechanica 226 (2015) 1641–1645.

[9] M. Farshad, On the shape of momentless tensionless masonry domes, Building and Environment 12 (1977) 81–85.

[10] C. Pesciullesi, M. Rapallini, A. Tralli, A. Cianchi, Optimal spherical masonry domes of uniform strength, Journal of Structural Engineering 123 (1997) 203–209.

[11] N. Cavalagli, G. Gusella, Structural investigation of 18th-century ogival masonry domes: From carlo fontana to bernardo vittone, Internationl Journal of Architectural Heritage 9 (3) (2015) 265–276.

[12] M. Pavlovic, E. Reccia, A. Cecchi, A procedure to investigate the collapse behavior of masonry domes: Some meaningful cases, International Journal of Architectural Heritage 10 (2016) 67–83.

[13] F. Foce, Milankovitch's theorie der druckkurven: Good mechanics for masonry architecture, Nexus Network Journal 9 (2007) 185–210.

[14] G. Cocchetti, G. Colasante, E. Rizzi, On the analysis of minimum thickness in circular masonry arches, Applied Mechanics Review 64 (5) (2011) 051002.1–22.

[15] N. Makris, H. Alexakis, The effect of stereotomy on the shape of the thrust-line and the minimum thickness of semicircular masonry arches, Archive of Applied Mechanics 83 (2013) 1511–1533.

[16] I. de Arteaga, P. Morer, The effect of geometry on the structural capacity of masonry arch bridges, Construction and Building Materials 34 (2012) 97–106.

[17] B. Riveiro, J. Caamaño, P. Arias, E. Snaz, Photogrammetric 3d modelling and mechanical analysis of masonry arches: An approach based on a discontinuos model of voussoirs, Automation in Construction 20 (2011) 380–388.

[18] B. Riveiro, M. Solla, I. de Arteaga, P. Arias, P. Morer, A novel approach to evaluate masonry arch stability on the basis of limit analysis theory and non-destructive geometric characterization, Automation in Construction 31 (2013) 140–148.

[19] P. Zampieri, M. Zanini, F. Faleschini, Influence of damage on the seismic failure analysis of masonry arches, Construction and Building Materials 119 (2016) 343–355.

[20] A. Zanaz, S. Yotte, F. Fouchal, A. Chateauneuf, Efficient masonry vault inspection by monte carlo simulations: Case of hidden defect, Case Studies in Structural Engineering 5 (2016) 1–12.

[21] L. Caporale, R. Luciano, L. Rosati, Limit analysis of masonry arches with externally bonded frp reinforcements, Computer Methods in Applied Mechanics and Engineering 196 (1–3) (2006) 247–260.

[22] E. Benvenuti, O. Vitarelli, A. Tralli, Delamination of frp-reinforced concrete by means of an extended finite element formulation, Composites Part B: Engineering 43 (2012) 3258–3269.

[23] A. Caporale, L. Feo, D. Hui, R. Luciano, Debonding of frp in multi-span masonry arch structures via limit analysis, Composite Structures 108 (2014) 586–865.

[24] E. Grande, G. Milani, Modeling of frp-strengthened curved masonry specimens and proposal of a simple design formula, Composite Structures 158 (2016) 281–290.

[25] C. Franciosi, Limit behaviour of masonry arches in the presence of finite displacements, International Journal of Mechanical Sciences 28 (7) (1986) 463–471.

[26] P. Clemente, Introduction to dynamics of stone arches, Earthquake Engineering and Structural Dynamics 27 (1998) 513–522.

[27] I. Oppenheim, The masonry arch as a four-link mechanism under base motion, Earthquake Engineering and Structural Dynamics 21 (1992) 1005–1017.

[28] M. DeJong, L. De Lorenzis, S. Adams, J. Ochsendorf, Rocking stability of masonry arches in seismic regions, Earthquake Spectra 24 (4) (2008) 847–865.

[29] N. Cavalagli, V. Gusella, L. Severini, Lateral loads carrying capacity and minimum thickness of circular and pointed masonry arches, International Journal of Mechanical Sciences 115–116 (2016) 645–656.

[30] L. Severini, Effects of shape and geometrical uncertainties on the static and dynamic behavior of the masonry arch, PhD dissertation, In partial fulfillment of the requirements for the degree of Doctor of Philosophy in Civil Engineering and Innovative Materials. Submitted to the Department of Civil and Environmental Engineering, University of Perugia (2017).

[31] P. Callaway, M. Gilbert, C. Smith, Influence of backfill on the capacity of masonry arch bridges, Proc. of the Institution of Civil Engineers: Bridge Engineering 165 (2012) 147–158.

[32] G. Milani, P. Lourenço, 3d non-linear behavior of masonry arch bridges, Computers and Structures 110–111 (2012) 133–150.

[33] A. Caddemi, G. Ricciardi, C. Sacc, Limit analysis of structures with stochastic strengths by a static approach, Meccanica 37 (2002) 527–544.

[34] A. Brencich, L. Gambarotta, E. Sterpi, Stochastic distribution of compressive strength: effects on the load carrying capacity of masonry arches, in: Proc. 5th International Conference on Arch Bridges, Madeira, Portugal, 2007.

[35] K. H. Ng, C. Fairfield, Monte carlo simulation for arch bridge assessment, Construction and Building Materials 16 (2002) 271–280.

[36] L. Schueremans, P. Smars, D. Van Gemert, Safety of arches - a probabilistic approach, in: Proc. 9th Canadian Masonry Symposium, Fredericton, NB, Canada, 2001.

[37] S. Rao, L. Berke, Analysis of uncertain structural systems using interval analysis, AIAA Journal 35 (4) (1997) 727–735.

[38] S. Rao, Description and optimum design of fuzzy mechanical systems., 1986.

[39] L. De Lorenzis, M. DeJong, J. Ochsendorf, Failure of masonry arches under impulse base motion, Earthquake Engineering and Structural Dynamics 36 (2007) 2119–2136.

[40] H. Alexakis, N. Makris, Limit equilibrium analysis and the minimum thickness of circular masonry arches to withstand lateral inertial loading, Archive Applied Mechanics 84 (2014) 757–772.